



Integrating microclimate modelling with building energy simulation and solar photovoltaic potential estimation: The parametric analysis and optimization of urban design[☆]

Chenhang Bian ^a, Ka Lung Cheung ^{a,b}, Xi Chen ^{b,*}, Chi Chung Lee ^{a,*}

^a Department of Construction and Quality Management, Hong Kong Metropolitan University, Ho Man Tin, Kowloon, Hong Kong

^b Department of Mechanical and Automation Engineering, The Chinese University of Hong Kong, Shatin, NT, Hong Kong

HIGHLIGHTS

- HDMR, Sobol sampling and bootstrapping strategies are coupled for feature extraction in microclimate modelling.
- An integrated multi-objective urban performance optimization workflow is proposed.
- Interaction between urban microclimate, building energy consumption, and solar energy utilization is explored.
- Correlation between building height and density with key urban performance indicators are revealed.
- Optimal urban block form is determined for urban energy efficiency and microclimate regulation.

ARTICLE INFO

Keywords:

Urban microclimate
Urban block form
Parametric modelling
Design optimization
Photovoltaic power potential

ABSTRACT

Key urban design factors of the meteorological condition, vegetation, urban block form, transportation and building design as well as their interaction need to be explored to regulate urban microclimate, building energy efficiency, and solar photovoltaic (PV) generation for enhancing the overall building/urban energy performance. This study first incorporates the High Dimensional Model Representation (HDMR), Sobol sampling and bootstrapping strategy to extract the most important factors for microclimate modelling. Then, a parametric modelling and design optimization framework is proposed to improve the overall building energy performance (i.e. building energy consumption and PV power generation) while mitigating local climate change (i.e. urban heat island effect) by exploring various urban block form designs. The integrated urban performance optimization platform is further demonstrated in a high-density district in Hong Kong. The research results demonstrate a significant correlation between building density (BD), building height (BH), photovoltaic power generation, and the urban heat island effect. Building height shows a strong positive correlation with accumulated urban heat island intensity (AUHII) ($R^2 = 0.4512$) and photovoltaic power generation ($R^2 = 0.6720$). Building energy consumption is found to be correlated with building density, with a correlation coefficient of 0.2052, but it is barely influenced by building height. From clustering analyses, optimal urban block designs are determined for different optimization objectives. The findings presented in this paper have important indication for sustainable urban form design.

1. Introduction

With the advent of urbanization in the post-pandemic era, energy shortages and climate change have brought greater challenges to

countries around the world. According to a report on the global construction industry at the United Nations Climate Conference held in Egypt in 2022 [1], the energy demand of the construction industry accounted for more than 34 % of the total in 2021, and energy-related carbon dioxide emissions accounted for 37 %. Official data indicate

[☆] The short version of the paper was presented at CUE2024, Shenzhen, China, May 11-13, 2023. This paper is a substantial extension of the short version of the conference paper.

* Corresponding author.

E-mail addresses: xichen002@cuhk.edu.hk (X. Chen), ccllee@hkmu.edu.hk (C.C. Lee).

Nomenclature

BIPV Building-integrated photovoltaics.	FAST Fourier Amplitude Sensitivity Test.
HDMR High Dimensional Model Representation.	CSDI Common Spatial Data Infrastructure.
BD Building density.	OP Occupation Permit.
BH Building height m.	$T_{u,h}$ Urban temperature °C.
AUHII Accumulated urban heat island intensity °C•hr.	$T_{r,h}$ Rural temperature °C.
UHI Urban heat island.	H Number of time-steps.
PVG Photovoltaic power generation kWh/m ² .	k Weather station index.
TMY Typical meteorological year.	c-Si Crystalline silicon.
UWG Urban Weather Generator.	Z_{MAX} Maximum value of the optimization objective.
EUI Energy use intensity kWh/m ² .	Z_{MIN} Minimum value of the optimization objective.
SALib Sensitivity Analysis Library.	S_A Normalized value of PVG.
iMOO The integrated multi-objective optimization.	S_B Normalized value of EUI.
SA Sensitivity analysis.	S_C Normalized value of AUHII.
UA Uncertainty analysis.	Sa The uncorrelated contribution of a parameter.
LSA Local sensitivity analysis.	Sb The correlated contribution of a parameter.
GSA Global sensitivity analysis.	ST The total contribution of a particular parameter.
OAT One-at-a-time.	EMSD Electrical and Mechanical Service Department.
	EEO Energy Efficiency Office.
	SEGI Solar energy generation intensity.

that the energy and the environmental impact of Hong Kong's building sector is significant, with electricity consumption accounting for over 90 % of the city's total consumption and carbon emissions reaching over 60 %, tremendously exceeding the global average [2]. Integrating renewable energy sources like solar power becomes crucial for achieving climate change mitigation goals and reducing building energy consumption in this context [3]. The energy use of buildings is influenced by a complex interplay of factors, including climate conditions, building characteristics, system efficiency, and occupant behavior, forming an interactive network between these factors and the buildings themselves [4]. The rising temperature and extreme weather not only exacerbate building energy consumption but also highlight the urgent need to shift towards renewable energy, enhance energy efficiency, and mitigate climate change [5]. In addition to global climate change, microclimate variations, such as the urban heat island (UHI) effect, affected by urban morphology and surface characteristics, cause higher temperatures in urban centers compared to surrounding suburbs [6,7]. Furthermore, the intensification of urban heat island effects and the rapid pace of urbanization present even greater challenges in reducing energy consumption in buildings, especially in cooling energy [8]. Therefore, by optimizing the building design, improving the energy efficiency, and promoting the use of renewable energy, the construction industry can make a significant contribution to creating a high-quality and low-emission built environment. Integrating these sustainable practices not only addresses environmental issues but also supports global efforts to mitigate the climate change and achieve sustainable urban development [9].

Traditional building energy simulations, often relying on typical meteorological year (TMY) data from rural weather stations, are increasingly deemed inadequate for capturing the complexities of urban environment and local climate dynamics. The Urban Weather Generator (UWG) is a simulation tool developed by Bueno et al. [10] to specifically study the interaction between the UHI effect and building energy consumption. It has been validated by numerous research studies in different cities, [11–14]. Despite UWG's ability to perform efficient urban microclimate modelling [15–17], it requires a large number of input parameters related to meteorology, urban characteristics, vegetation, and traffic conditions. Sensitivity analysis is needed to identify the most important parameters and reduce the input dimension, allowing urban designers to make more efficient decisions to impact the model outputs [18]. Several studies have applied UWG in diverse urban contexts to better understand parameter influences. For instance, Nakano et al. [19] conducted a sensitivity analysis at MIT in the USA and

identified four key factors affecting the urban heat island effect, improving prediction accuracy by approximately 15 %. Xu et al. [20] conducted a study on 10 input parameters of UWG primarily related to urban morphology, finding that the location of open spaces, distribution of high-rise buildings, layout of land parcels, and building type significantly influence building energy consumption and solar potential. Aydin et al. [21] applied Sobol's sensitivity analysis method and Spearman correlation analyses to nine parameters in the UWG model, finding that in Singapore, the building density, podium density, and land parcel area have the greatest impact on UHI. Their analysis showed that strategic planning could lower annual UHI intensity by up to 30 % through specific design modifications. In a tropical climate, Litardo et al. [22] used UWG for microclimate modelling in Ecuador, revealing that urban morphology and anthropogenic heat are essential UHI drivers, with targeted mitigation strategies reducing cooling energy consumption in residential buildings by 30–70 %. For numerous cities worldwide, morphological parameters are the most critical factors affecting urban climate and building energy [6]. Despite these efforts, a gap remains in developing simplified models to reduce complexity and input requirements while maintaining accuracy. Further research is needed to examine UWG input parameters and enhance its applicability in different urban morphologies. From above studies, it can be clearly seen that the layout and design of building complexes have a significant impact on urban microclimates and building energy consumption [23]. The coupling of urban microclimate with building energy models has attracted wide attention in recent years [24], promoting more accurate information exchange between the peripheral environment and building energy simulations.

In recent years, building integrated photovoltaics (BIPV) and zero-energy buildings have become a hot spot in sustainable urban development. BIPV has great application potential in urban areas [25], even in a high density city with limited land space like Hong Kong, where large building envelope areas remain unutilized [26]. This provides Hong Kong with a distinct advantage in promoting the use of renewable energy and achieving its carbon neutrality goals. Studies have already been conducted on the integration of BIPV with building exterior walls [27], windows [28], and roofs [29], etc. PV surfaces have a high solar absorption rate, allowing them to convert solar radiation into electrical energy, whereas the high absorptance may intensify the UHI effect due to their low reflectivity and thermal diffusion properties [30]. Therefore, it is crucial to consider the comprehensive relationships between urban microclimate, building energy consumption, and solar energy utilization. For instance, Wu et al. [31] developed a genetic algorithm-based

parametric design approach for nearly zero-energy high-rise buildings, achieving higher solar photovoltaic utilization potential. Yet, this work was limited to single-building optimizations and did not consider surrounding urban morphology. Liu et al. [32] analyzed residential blocks in a city of China, revealing that optimized urban form can significantly improve building energy efficiency and solar energy potential. However, the study primarily focused on the block form without integrating other urban microclimate effects. Li et al. [33] explored the impact of urban morphology on building energy modelling using spatial proximity analysis and machine learning. Although insightful, this study lacked an assessment of solar energy applications within varying morphological contexts. Additionally, Hadavi et al. [34] investigated how urban configuration and density affect both climate and energy use in building systems. While their findings highlighted density's role in modifying local climates, they focused primarily on energy aspects, without delving into solar energy utilization. Many studies, like those by Wu and Zhang et al. [35], focus on low-density urban configurations, often neglecting the intricate inter-building effects that are crucial for accurate microclimate modelling. Tian et al. [36] further assessed the solar potential of building roofs and façades at the urban block scale but did not address UHI effects or overall energy consumption. Wang et al. [37] proposed an integrated framework merging urban morphology with low-energy design, utilizing data-driven methods. Though comprehensive, the study did not explicitly address photovoltaic potential across high-density urban layouts.

From the above introduction and literature review, it is evident that few studies comprehensively explore the impacts of urban microclimate, building energy consumption, and solar energy utilization. These topics are typically addressed in isolation. Furthermore, research on optimization urban block morphology, considering the complex interactions between urban morphology, local climate, and energy performance, remains insufficient. Most studies focus on low-density urban areas, often neglecting the complex inter-building effect in microclimate modelling.

To address above research gaps, particularly in the context of high-dimensional models, the present study developed a robust sensitivity analysis tool for microclimate modelling to extract the most important urban design parameters affecting the UHI effect. By identifying the key drivers of the UHI, urban planners and designers can better understand how to mitigate the negative impacts of local climate change through strategic interventions. Subsequently, a multi-objective urban block morphology optimization workflow is proposed to explore the influence of urban block form design on improving overall urban energy performance and mitigating local climate change. By optimizing block morphology, the goal is to find design solutions that not only reduce building energy consumption but also maximize the potential of solar energy utilization within the urban environment. This research provides specific urban morphology optimization strategies for subtropical high-density urban environments, thereby enhancing the understanding of the integrated relationships between urban microclimate, building energy consumption, and solar PV potential, and promoting the development of sustainable urban form design. The original contribution of this work lies in the following aspects: (1) Extraction of key urban design parameters affecting the urban heat island effect using a robust global sensitivity analysis method integrating HDMR, Sobol sampling and bootstrapping. (2) Proposing an integrated parametric modelling and design optimization framework to optimize urban energy (including building energy consumption and photovoltaic power generation) and mitigate urban heat island effect. (3) Exploring the correlation between identified key urban design factors as well as urban energy and thermal environmental indicators. (4) Determining the optimal block design for high-density subtropical cities under different optimization objectives, and forming foundations for sustainable urban design and renovation strategies.

The rest of the paper is organized as follows. Section 2 introduces the research framework of sensitivity analysis, parametric modelling and

optimization, as well as statistical analyses. Section 3 presents the key modelling results, statistical analyses, and their correlation with existing research. Finally, conclusions, limitations, and future work are summarized in Section 4.

2. Research design and methodology

Fig. 1 illustrates the overall research design of this study with four stages: microclimate simulation and sensitivity analysis, urban block form modelling, parametric modelling and integrated urban performance evaluation, and post-processing statistical analysis.

In Stage 1, 18 influencing factors related to urban characteristics and vegetation coverage are selected as key urban design input parameters for sensitivity analysis and microclimate modelling using the urban weather generator (UWG). The Sensitivity Analysis Library (SALib) is then utilized to conduct a high-dimensional model representation (HDMR) sensitivity analysis to identify key impact factors on the urban microclimate. Furthermore, bootstrapping is applied to generate more reliable sensitivity indices when dealing with high-dimensional input data and complex models. In Stage 2 and 3, ArcGIS and QGIS are used to extract building information from the real city model and build the ideal neighborhood block model in Rhino. Each model involves calculating microclimate, building energy consumption, and photovoltaic generation, implemented with Ladybug, Honeybee, and Dragonfly plugins integrated into Grasshopper. The microclimate simulation results of urban blocks are directly coupled with building energy simulations to improve modelling accuracy. In Stage 4, polynomial regression analysis is employed to investigate the links between the urban design parameters and the multiple performance objectives. Additionally, clustering analysis is used to group the design solutions according to their characteristics and overall performance. Finally, the integrated multi-objective optimization (iMOO) model is applied to determine optimal design solutions that can simultaneously regulate urban energy performance and local climate.

Fig. 2 shows the entire simulation process in Grasshopper, including the generation of the ideal urban block and simulation of building energy consumption, solar radiation, and urban microclimate.

2.1. Study area and climate description

In this research, a typical high-density district in Hong Kong is studied to implement the proposed sensitivity analysis and integrated performance optimization framework. Hong Kong hosts 7.187 million people on only 1105.6 km² of land, with a population density as high as 6650 people/km² [38]. Mong Kok, located in the center of the Kowloon district, has an extremely high population density. It is a mixed commercial and residential area where new skyscrapers, old tenement buildings, bustling streets, and food stalls coexist, making it one of the world's largest urban landscapes.

The weather in Hong Kong is subtropical and classified as climate zone 2 according to ASHRAE standards [39]. Urban climate is a crucial factor that affects urban energy consumption and the micro-environment. Variables such as air temperature, relative humidity, wind speed, and wind direction influence the thermal conditions of buildings and heat transfer across building surfaces, ultimately impacting building energy consumption. Hourly weather data used in the baseline for EnergyPlus simulations come from the typical meteorological year (TMY) in Hong Kong [40]. TMY weather data are compiled based on individual months from multiple years over a 20 to 30-year period to represent the long-term average climatic conditions. Through a preliminary analysis of the dry-bulb temperature, wind speed and direction, and solar radiation from TMY data, Hong Kong is characterized by the high cooling demand, predominant east and west wind in summer, and sufficient solar radiation throughout the year. The analysis highlights the potential benefits of solar energy utilization, particularly for south-facing buildings in Hong Kong. More detailed

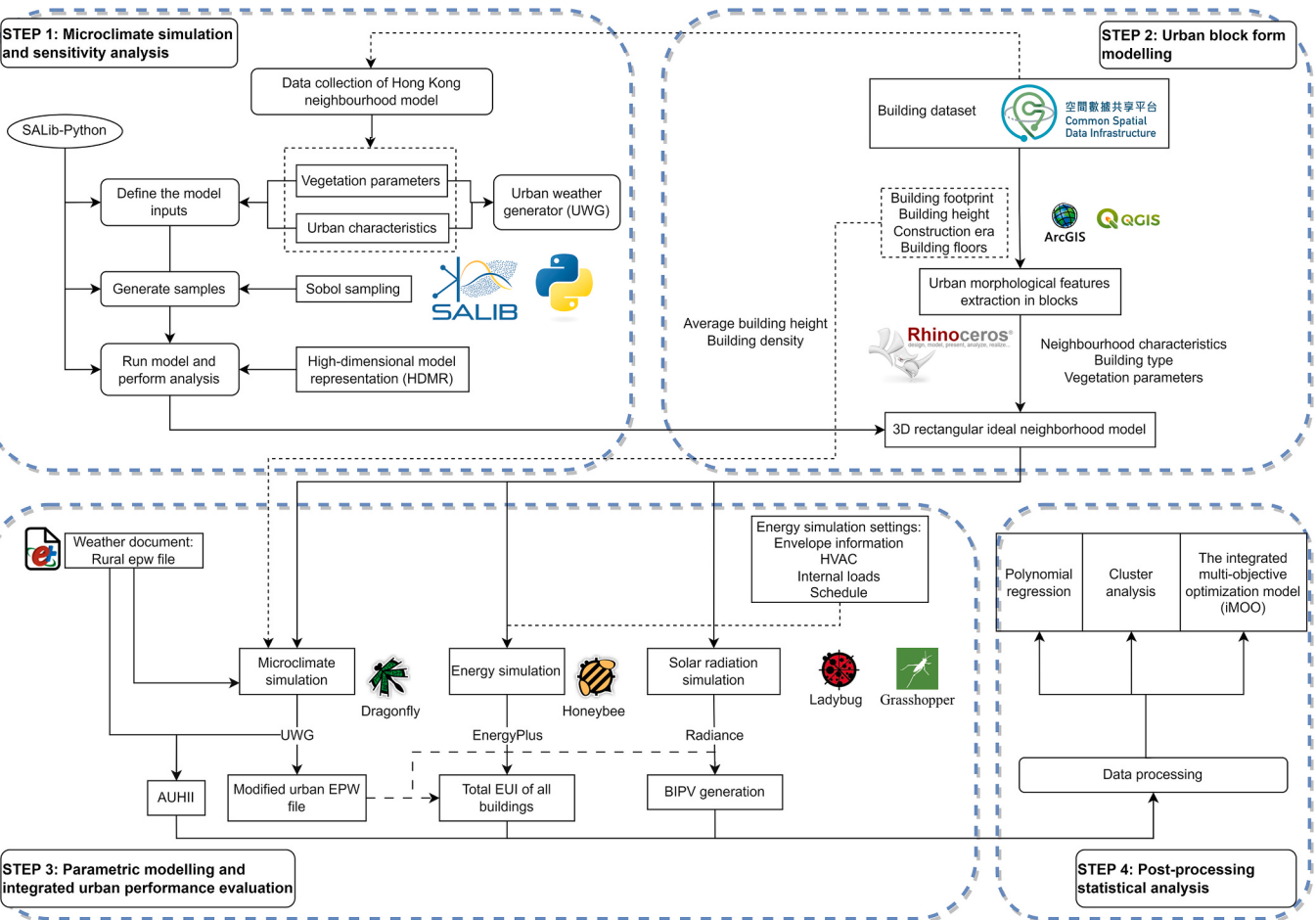


Fig. 1. The overall flow chart of this study.

analyses can be found in Appendix A.

2.2. Sensitive analysis to extract key urban design features for microclimate modelling

Sensitivity analysis (SA) is a method that studies how model predictions are influenced by the variation of model inputs. By examining the sensitivity and correlation between variables, important features in a data set can be identified, leading to reduced input data dimension and higher prediction efficiency. SA can be categorized into two main types: local sensitivity analysis (LSA) and global sensitivity analysis (GSA) [41]. LSA methods focus on specific points in the parameter space and involve comparing outputs to known “baseline” values. Commonly used LSA methods include One-at-a-time (OAT) and derivative-based local methods. However, LSA does not consider interactions between multiple parameters, and the computational cost increases when high-order and nonlinear effects are considered [42].

On the other hand, GSA considers all dimensions of the model by varying all parameter values simultaneously. GSA methods [43,44] typically include regression-based, screening-based, and variance-based methods. By comprehensively considering the interactions between all parameters, GSA provides a more robust description of model uncertainty. However, the computational cost of GSA can be high due to the large parameter space, making it challenging to use in practical applications. To address this issue, sampling methods can be employed to ensure that the parameter space is adequately represented with manageable computational costs.

SALib [45,46] is an open-source Python library that facilitates sensitivity analysis [45,47,48]. It offers various sensitivity analysis

methods, such as Sobol [49], Morris [50], Fourier Amplitude Sensitivity Test (FAST) [51], and High Dimensional Model Representation (HDMR). Among these methods, Sobol and Morris are suitable for nonlinear models. Sobol can quantify first-order and higher-order sensitivities, but it has a high computational cost and does not consider parameter correlations. Morris has a low computational cost but cannot provide a quantitative analysis of sensitivity. FAST, although applicable to both monotonic and non-monotonic models, has a relatively low computational cost but is not suitable for computing higher-order sensitivities and does not consider parameter correlations. For high-dimensional models with a large sample size, HDMR becomes very useful. HDMR [42,52] adopts a metamodeling method to improve variance-based SA methods like Sobol and FAST. Initially proposed by Rabitz et al. [53], HDMR explores input-output relationships in complex models with a large number of variables. It utilizes least squares regression to reduce the required number of samples, thereby decreasing the number of function (model) evaluations. It can also elucidate the correlations among model inputs by treating the primary influence as a combination of contributions from the structure (uncorrelated) and correlations. Therefore, according to the research objectives and data characteristics of this article, the HDMR framework is used for simulation and analysis.

Eighteen input parameters of the Urban Weather Generator (UWG) related to urban design are selected to quantify their impact on the microclimate. Since a substantial change in land properties and functions is not reasonable for a highly developed urban area, the variation range of each parameter was defined based on their realistic distribution in Hong Kong [17]. Subsequently, SALib was called using a developed Python script to read and create input parameter samples for running UWG simulations. The outputs of the UWG simulations were collected to

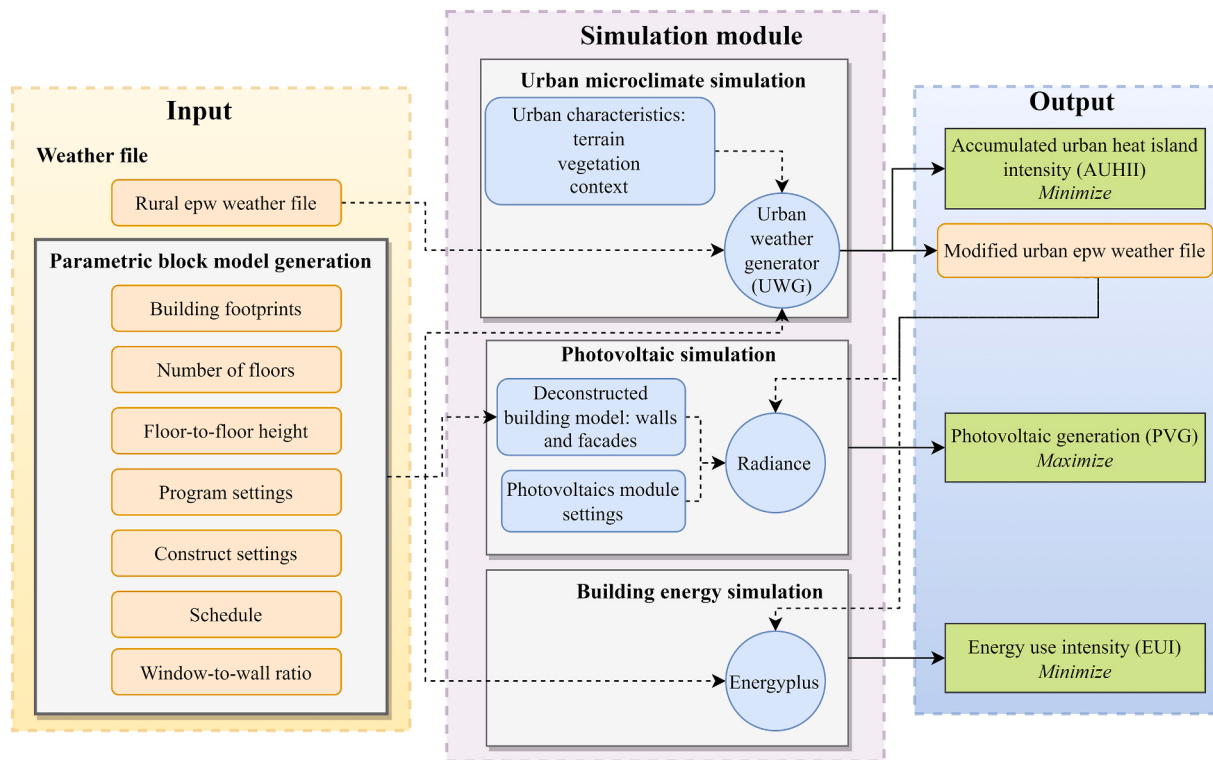


Fig. 2. Flowchart for ideal urban block model generation and integrated modelling of microclimate, building energy consumption, and solar potential in grasshopper.

quantify the impacts of different urban design parameters on the local thermal environment with specific SALib algorithms. Sufficient parameter samples were necessary to ensure the convergence of the sensitivity analysis process. In this study, a total of 2052 simulations were conducted to balance analysis accuracy and computational cost. UWG, developed by Bueno et al. [10], consists of four interconnected modules: a rural station model, vertical diffusion model, urban boundary layer model, and urban canopy-building energy model. Three predefined building models in the UWG tool are used to simulate energy consumption for a typical mid-rise apartment (0.35 ratio), a large office building (0.35 ratio), and a small office building (0.3 ratio) from the 1980s to represent building complexes in the study area described in Section 2.1. Table 1 provides a list of the main research variables and their corresponding ranges of variation.

2.3. Parametric modelling of urban block forms

2.3.1. Urban form extraction

Fig. 3 displays the aerial view of the entire Mong Kok area in Hong Kong and 3D model of the street block. The building footprint and other data used in this study were sourced from Hong Kong's Common Spatial Data Infrastructure (CSDI). The building type and number of floors were obtained from Google. The construction year was obtained from the Occupation Permit (OP) in BRAVO-online of the Hong Kong Buildings Department. Initially, the collected map data was imported into ArcGIS 10.7 for calculating the building heights. Subsequently, the buildings and roads were vectorized into ESRI shape files (SHP files) and imported into Rhino and Grasshopper to form the urban district model.

2.3.2. Hypothetical block form model generation

Based on the actual road grid scale in Mong Kok, this study selects a 195 m × 195 m block as the ideal size, which is further divided into a 3 × 3 grid to generate 9-unit plots (as seen in Fig. 4). The boundary line of the unit plot has a setback of 5 m from the road centerline. The dimension of the unit plot is 55 m × 55 m, and it is assumed that only

Table 1
The main research parameters and scope for the UWG model.

Variable	Physical Meaning	Range of Design Space
runVegCover	Fraction of the rural ground covered by vegetation	[0.3–1]
latTree	Fraction of the heat absorbed by trees that is latent	[0–1]
latGrass	Fraction of the heat absorbed by grass that is latent	[0–1]
albVeg	Vegetation albedo	[0–1]
vegStart	The month in which vegetation starts to evapotranspire	M_s
vegEnd	The month in which vegetation stops evapotranspiring	M_e
treeCover	Fraction of the urban ground covered in trees	[0–1]
grassCover	Fraction of the urban ground covered in grass/shrubs only	[0–1]
sensAnth	non-building sensible heat at street level	2000.0, 8000.0
cRoad	road volumetric heat capacity (J/m ³ K)	[0–1]
kRoad	road pavement conductivity (W/m K)	[0–1]
dRoad	road pavement thickness (m)	[0–1]
albRoad	road albedo	[0–1]
charLength	dimension of a square that encompasses the whole neighborhood	[700–1300]
h_mix	Fraction of building HVAC waste heat set to the street canyon	[0.0–1.9]
verToHor	Urban area vertical to horizontal ratio	[0–1]
bldDensity	Urban area building plan density	(0–1)
bldHeight	Average building height (m)	(0–120)

one building type unit can be placed per plot.

2.3.3. Extraction of building types

According to the land use distribution in Hong Kong [54], building types can be divided into residential, commercial, industrial, and office buildings. Since there are many residential buildings and commercial shopping centers in Mong Kok, this study mainly constructs a rich block

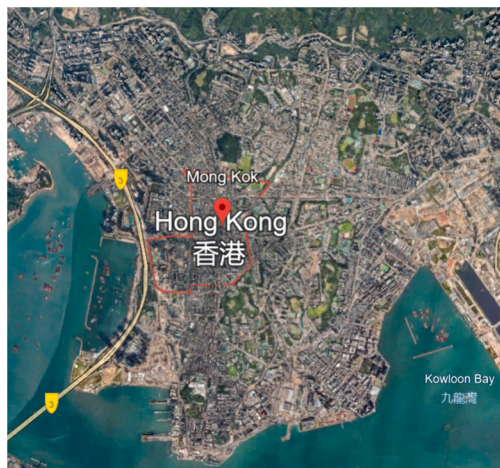


Fig. 3. Aerial view of Mong Kok and 3D model of the street block.

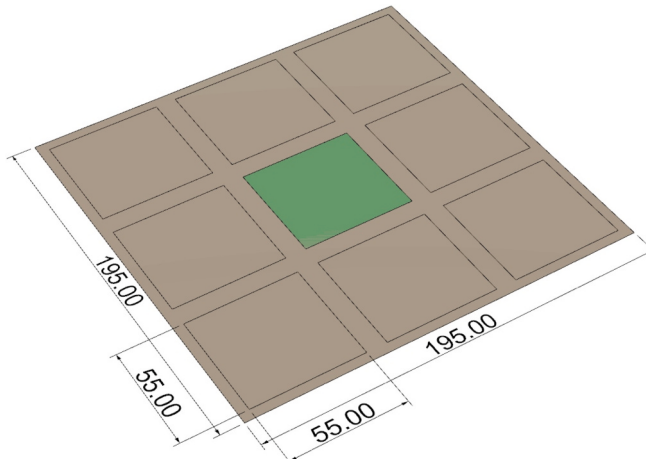


Fig. 4. Illustration of an ideal urban block.

form based on residential, commercial, and office buildings. Through field research and satellite image recognition, and based on the description of building characteristics by the Housing Department [55] and some researchers [56,57], a total of eight common building types were identified. Five of these were residential buildings, numbered R-1 to R-5; there were also two office buildings, numbered O-1 and O-2, and one commercial building, numbered M-1. The floor height was uniformly set to 3 m, and the simulated building height was calculated by multiplying the actual number of floors by the floor height. Table 2 and Table 3 shows the schematic diagram and detailed description of the actual form of the eight buildings.

2.3.4. Key urban design parameters

Building density (BD) (See Eq. (1)) describes how close buildings are allocated in a certain urban area. In highly dense areas, buildings are often located closer to each other, with reduced separation. The building height (BH) represents the average value of all buildings in an urban block, normalized by the total building footprint.

$$BD = \sum_{i=1}^n f_i / A_s \quad (1)$$

where f_i refers to the footprint of building i , A_s refers to the site area of the urban block.

2.4. Integrated urban performance evaluation

2.4.1. Performance indicators

As discussed in the previous sections, this paper focuses on the comprehensive simulation of the urban heat island effect, building energy consumption, and solar energy potential of constructed urban blocks within the study area. Therefore, three specific performance indicators are selected for this study: accumulated urban heat island intensity (AUHII), energy use intensity of all buildings (EUI), and PV generation (PVG).

The primary inputs to the Urban Weather Generator (UWG) are urban morphological information and rural weather files. The input urban morphological information includes the climate zone (2 A for Hong Kong), vegetation details (such as tree and grass coverage), building features (including the building type, air conditioning systems, window to wall ratio, mean building height, and building coverage), and urban characteristics (such as geometry and heat transfer properties including albedo, emissivity, thermal conductivity, and volumetric heat capacity). In this study, the mean building height, building coverage, and façade-to-site ratio vary among different blocks. For other parameters, the default values in UWG models are adopted and kept constant for all blocks. Urban heat island intensity (UHII) is defined as the temperature difference between urban blocks and a reference rural weather station as a traditional indicator of the urban heat island effect. However, since temperature is a transient and variable climate condition, UHII usually changes with time. In this study, the accumulated urban heat island intensity (AUHII) proposed by Cui et al. [58] is used to describe the cumulative urban heat island intensity effect within a certain period. The larger the AUHII (See Eq. (2)), the more significant the difference between the urban and rural area.

$$AUHII = \sum_{h=1}^H [T_{u,k,h} - \min(T_{u,k,h}, T_{r,k,h})] \quad (2)$$

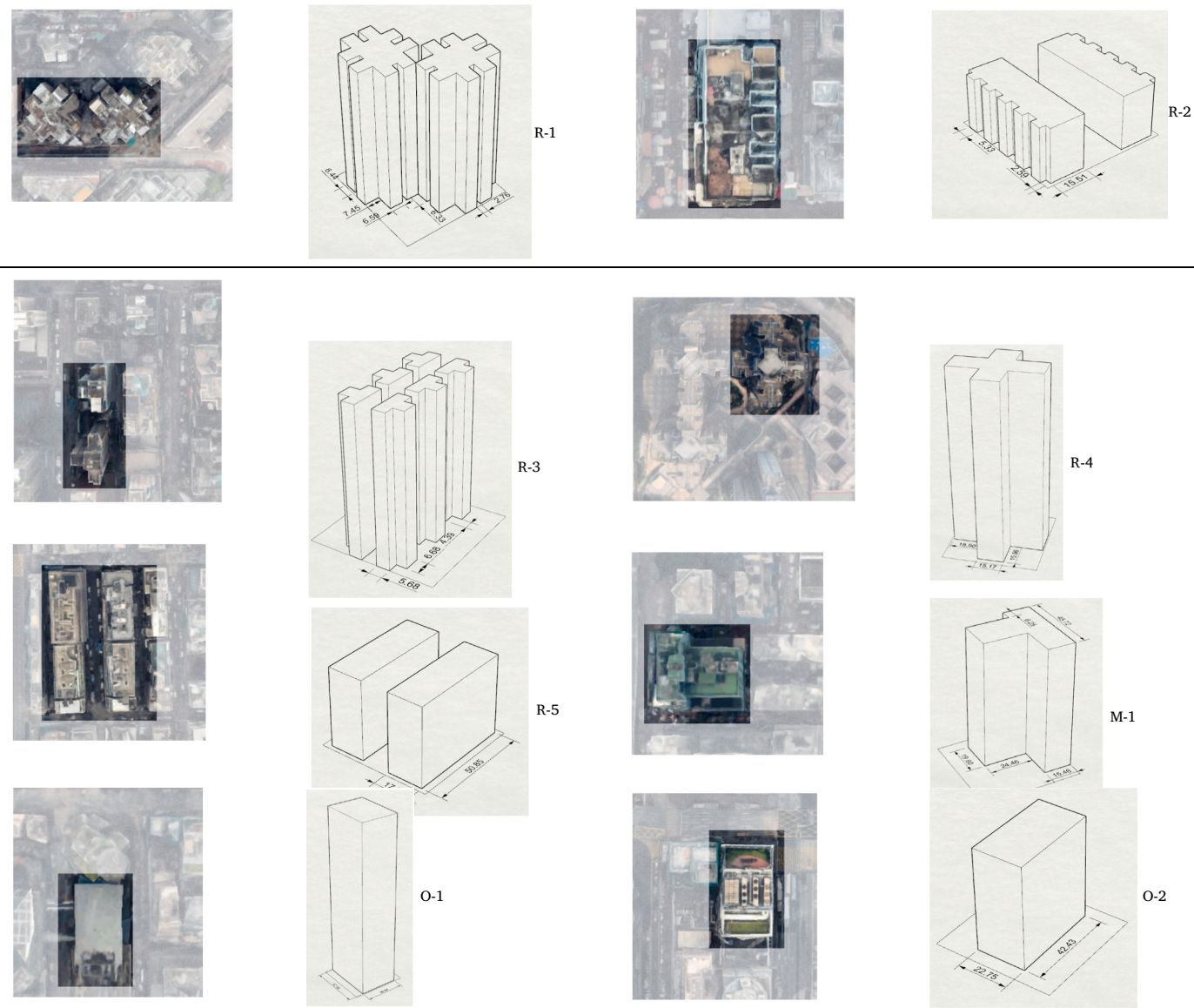
where $T_{u,h}$ refers to the urban temperature at time-step h , $T_{r,h}$ refers to the rural temperature at time-step h . H is the number of time-steps and k is the weather station index.

Building energy simulation is conducted using Honeybee to operate the EnergyPlus engine. EnergyPlus is a holistic building energy simulation program developed with the support of the US Department of Energy and widely used in academic and engineering applications [59]. In this paper, the annual building energy intensity calculation is performed for buildings across the entire block. To ensure acceptable simulation time, each floor is set as one thermal zone.

Photovoltaic power generation (PVG) was calculated based on the amount of available solar radiation on the panel surface. The specific

Table 2

Typical floor plan of 8 building prototypes.

**Table 3**

Description of the selected eight building types and a grass land.

No.	Building footprint area (m^2)	Height (m)	Number of floors
R-1	1296	75	25
R-2	1734	24	8
R-3	713	63	21
R-4	1372	108	36
R-5	1761	63	21
O-1	2040	180	60
O-2	961	48	16
M-1	1185	72	24
G-1	3025		

solar radiation calculation is simulated using the Radiance engine operated by the Ladybug plugin. Annual rooftop and façade photovoltaic generation are used to represent the solar potential of the block. Crystalline silicon (c-Si) photovoltaic panels are selected with a reasonable assumption of the conversion coefficient at 15 %, and DC-AC conversion coefficient at 85 % [60]. According to the actual situation, the coverage rate of roof photovoltaic panels is defined as 90 % to reflect

the installation constraint. It is important to note that the solar PV generation mentioned in this paper does not consider the energy loss from power storage and distribution or different array configurations.

2.4.2. The integrated multi-objective optimization (iMOO) model

To determine the optimum solution while considering the trade-off between different objectives, the integrated multi-objective optimization (iMOO) model developed by Koo et al. [61] is adopted to rank modeled design scenarios.

The process of standardizing the optimization objective function involves transforming the objective values to range between their upper and lower limits. In this study, the single objective optimization process is initially conducted for each objective, and then all the objective functions are normalized using the Eq. (3) [62].

$$S_A = (Z_A - Z_{\text{AMIN}}) / (Z_{\text{AMAX}} - Z_{\text{AMIN}}) \quad (3)$$

where S_A is the normalized value of Z_A , Z_{AMAX} is the maximum value of the optimization objective A and Z_{AMIN} is the minimum value of the optimization objective A.

Finally, the fitness function is defined as the iMOO score, which is

used to identify the optimal design solution with the lowest iMOO score. Considering that multi-objective optimization cannot minimize all objective functions simultaneously, the “Weighted Euclidean Distance” method is used to balance multiple optimization objectives of maximizing PVG, minimizing EUI, and minimizing AUHII, thereby obtaining the ultimate optimal solution (See Eq. (4)).

$$\text{Fitness Function} = \sqrt{(1 - S_A)^2 / 3 + (S_B - 0)^2 / 3 + (S_C - 0)^2 / 3} \quad (4)$$

where S_A , S_B and S_C represent the normalized values of the optimisation objectives PVG, AUHII and EUI, respectively; And the value of the fitness function represents the iMOO score.

3. Results and discussion

3.1. Sensitivity analysis for microclimate modelling

Sobol sampling is first applied to generate sample points by binning the input parameters and using low-order polynomials to approximate the model output. It can provide global sensitivity indicators and is suitable for exploring the complex relationship between the input parameters and output. Therefore, the Sobol sampler is used to sample all independent variables to generate uniform random distribution results. A total of 1024 sample points were generated.

Fig. 5 illustrates the distribution of generated samples for each input parameter from UWG. It can be seen that charLength, sensAnth, grassCover, treeCover, vegStart, vegEnd, albVeg, and latGrss show a roughly

uniform probability distribution, while the others are close to a normal distribution. BldHeight is sampled between 0 and 125, and shows the highest probability around 62.5, reflecting the diversity of building heights in the study area. BldDensity ranges from 0 to 1, and is similar to a normal distribution. Moreover, verToHor, h_mix, albRoad, dRoad, kRoad, cRoad also have similar distributions, indicating their high correlation. In addition, compared with the current popular analysis methods, such as Sobol, Morris, the distinctive characteristics of HDMR is to decouple the input variables and transform a high-dimensional problem into a low, middle, or combination of middle-dimensional functions. Therefore, a High Dimensional Model Representation (HDMR) is used to obtain a more robust sensitivity analysis result with a limited number of samples. HDMR parameter regression analysis is mainly used to estimate the coefficients or weights associated with each input parameter in the model, identify the optimal fit between the input parameters and the corresponding coefficients, and determine the most influential parameters. The model output of HDMR exhibits a non-linear relationship with input parameters such as building height and building density (Fig. 6). ST stands for the studied parameters (urban height, density etc.)

To further evaluate the fitting performance and stability of all indicators, Bootstrap analyses are performed using the same sample size as the original dataset [52]. The actual data points are consistent with the ideal linear relationship, indicating that the sensitivity indices obtained are of high accuracy.

Sensitivity indices generated by HDMR are shown in Fig. 7. The Sa of building density is significantly higher than those of other input

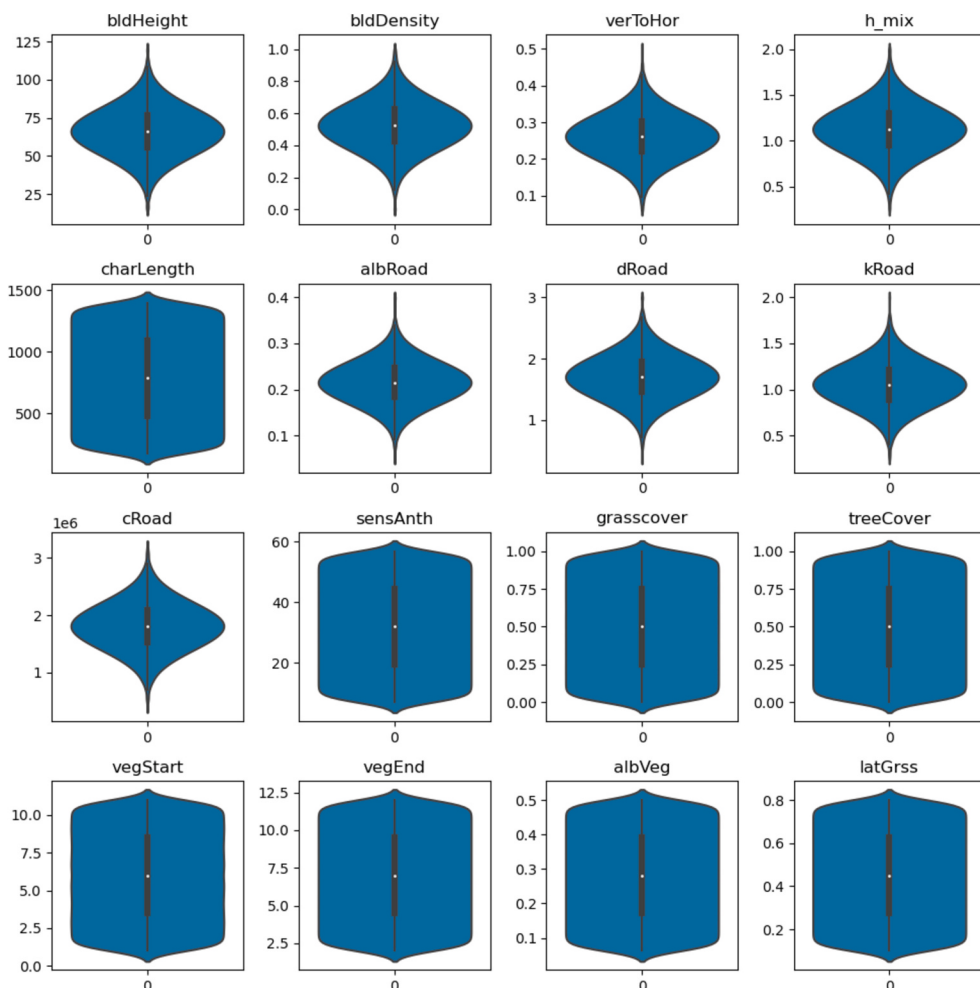


Fig. 5. Violin plots of the distribution of each input factor for the sample.

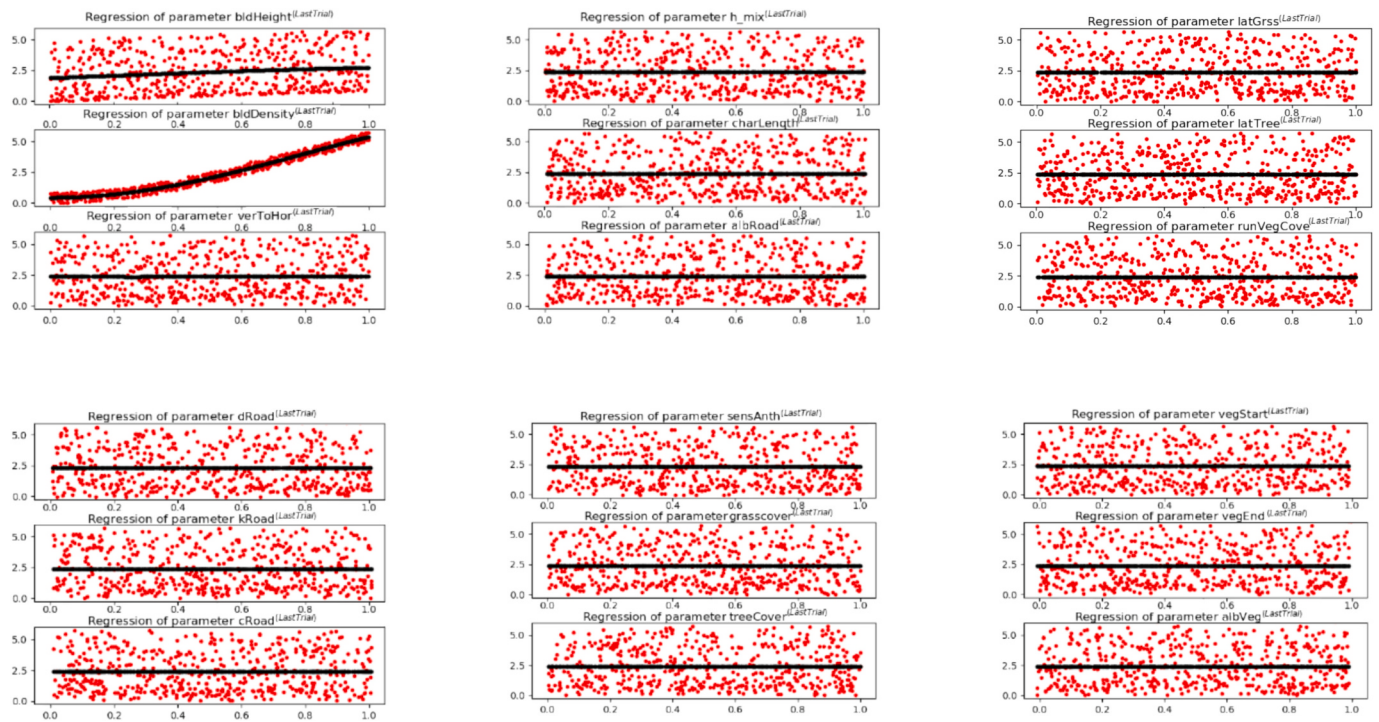


Fig. 6. The results of HDMR parameter regression analysis.

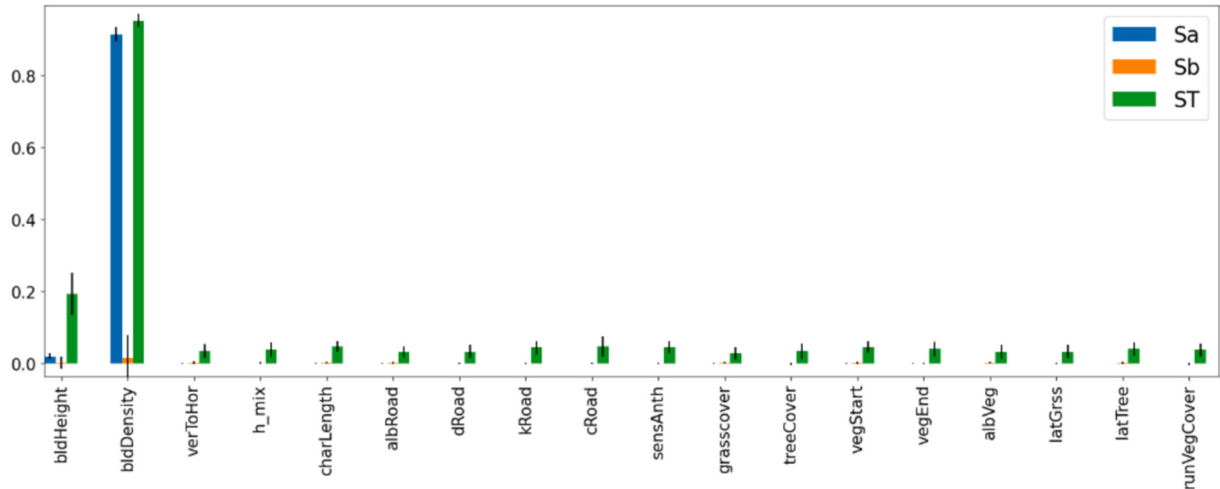


Fig. 7. HDMR sensitivity analysis indexes. (Sa represents the uncorrelated contribution of a parameter; Sb represents the correlated contribution of a parameter; ST represents the total contribution of a particular parameter [53]).

parameters, indicating that the model output result is particularly sensitive to building density. Building height is the second most significant input following building density. When considering the correlation with other input parameters, it can be observed that Sb values of building height and building density are slightly higher, indicating high relative contributions. In terms of the overall sensitivity represented by ST, building density and height remain the top two. The sensitivity results obtained in this study are consistent with those of existing urban heat island studies as summarized in Table 4.

3.2. Impact of block form design on integrated urban performance

Based on the generated urban block designs and modeled performance indicators, polynomial regression is employed to investigate the impact of urban design on the three optimization objectives: building

energy consumption, urban heat island effect, and solar power generation.

3.2.1. Correlation analysis between optimization objectives and urban morphological parameters

A total of 200 cases with different block form designs were simulated, and the annual performances of the urban blocks are presented in Fig. 8. The performance indicators include total photovoltaic generation on the rooftop and façades of all buildings (PVG), urban building energy intensity (EUI), and accumulated urban heat island intensity within the studied area (AUHII). The mean values for PVG, AUHII, and EUI are estimated as 54.27 kWh/m², 263.75 °C•hr, and 379.7 kWh/m², respectively. One case exhibited a significantly higher EUI value of 868.26 kWh/m², which is considered an outlier and excluded from subsequent analyses.

Table 4
Research in related literature.

Year	Location	Method	Important Factors
2012 [63]	France	SA: compare variations between two files	Urban density, height
2019 [64]	France	Randomize sampling and plotting	Urban density, height
2016 [65]	South-American	Simulation studies	Urban density, height
2022 [66]	Germany	Monte Carlo-based sensitivity analysis (SA) and uncertainty analysis (UA)	Urban density, height
2014 [67]	Italy	ENVI-MET	Urban density, height
2012 [68]	Hong Kong	ENVI-MET	Urban density, height
2016 [69]	Hong Kong	ENVI-MET	Urban density and green coverage

The annual building energy use of 200 blocks was simulated using EnergyPlus. The simulation result shows that the yearly average EUI of the mixed block is 379.7 kWh/m². Existing research also identified the annual EUI of buildings in Hong Kong as 362 kWh/m² in 2018 [70]. Additionally, actual electricity bills from 2012 to 2014 indicated that the EUI range for buildings in Hong Kong was between 78 and 530 kWh/m² [71]. A comparison of these data shows that the simulated EUI is within a reasonable range. Furthermore, the breakdown of energy consumption by end-uses in the simulated urban blocks is shown in Fig. 9. Cooling energy consumption accounts for the largest portion (71 %), followed by indoor lighting (13 %) and electrical equipment (10 %). The water and heating system consume the least energy, each accounting for less than 5 %. Our energy use pattern closely aligns with the findings of Jing et al. [71], where cooling and lighting accounted for 68 % and 14 %, respectively, indicating that cooling and lighting systems are the

primary contributions to energy consumption in Hong Kong buildings.

The accumulated urban heat island intensity (AUHII) is used to describe the cumulative urban heat island intensity effect over a certain period. Although it is less frequently mentioned in existing research, this concept is crucial as it provides deeper understanding of the cumulative impact of the urban heat island phenomenon over time and serves as a key indicator for assessing the long-term impact on urban microclimates [72]. Taking the block model as an example, the UHII of each season in this study was simulated and compared to validate the accuracy of the simulation results. Table 5 lists the seasonal UHII values obtained in this study and those from Ma et al. [73]. These results show very small differences, indicating that our simulation results provide a reasonable representation of UHII across seasons. The slight variations may be attributed to differences in input data between the studies.

A recent study by Liang et al. [74] estimated that the PV power generation in Hong Kong ranges from 50.7 to 65.2 kWh/m². Although vertical photovoltaic panels do not meet the optimal tilt angle requirements, they are both technically and economically feasible [75]. Given different installation conditions and scales, the simulated photovoltaic power generation range of 50–60 kWh/m² in our research is also reasonable compared to existing literature.

Fig. 10 illustrates the range of simulated energy consumption, with most total EUI values falling between 200 and 500 kWh/m², and some extreme values exceeding 600 kWh/m², indicating that such block morphologies are unfavorable for sustainable city development. Fig. 11 shows the contribution of Building-integrated Photovoltaic (BIPV) power generation to EUI reduction. BIPV power generation can account for up to 43.73 % of energy consumption, though some block forms cause severe inter-shading, resulting in low solar potential (as low as 2.96 %) on their exterior walls and roofs.

Unlike the traditional linear regression, polynomial regression [76] considers the non-linear relationships between variables, so its modelling accuracy is better. Considering the two-sided nature of the effects of

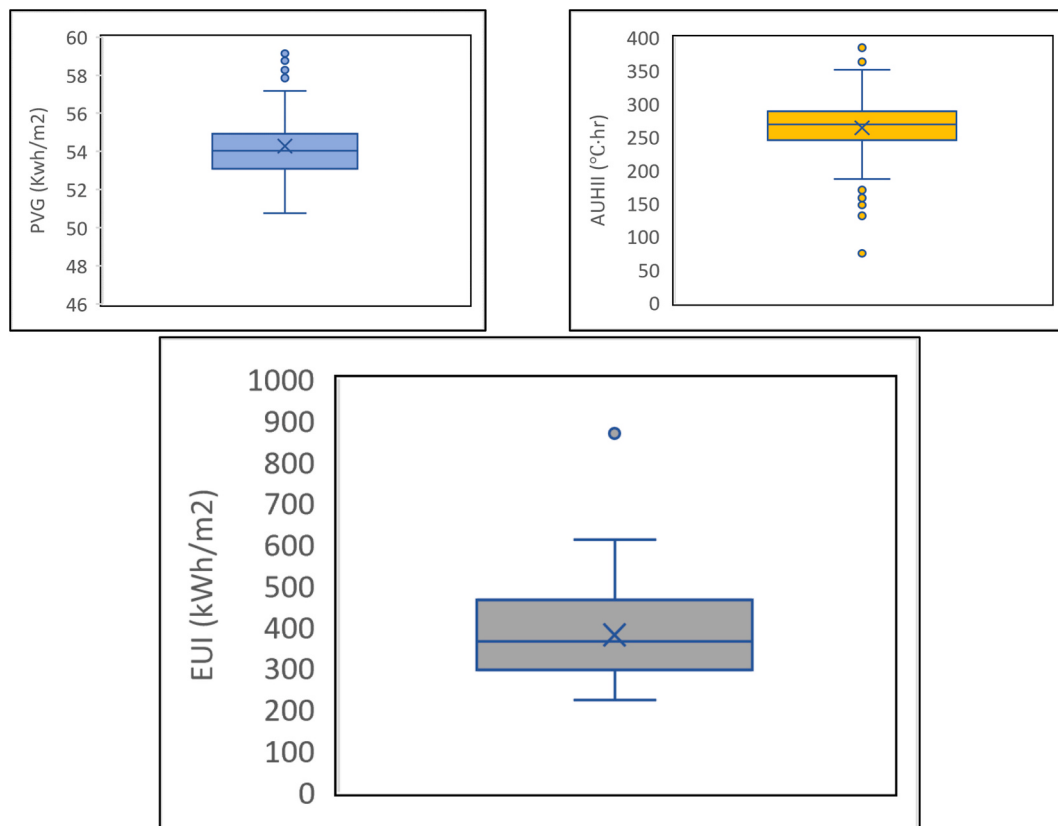


Fig. 8. Box plot of three optimization objectives PVG, AUHII, EUI.

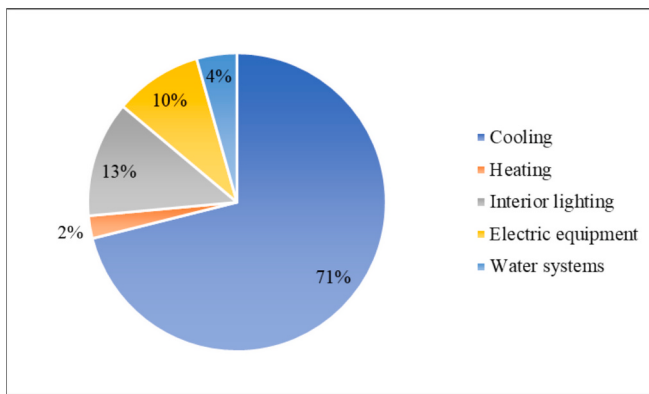


Fig. 9. Distribution of energy consumption in different components of the building.

Table 5
Comparison of simulated UHII for different seasons.

	Urban heat island intensity (UHII) / °C		
	Winter	Transitional Seasons	Summer
Simulation results	1.4	0.75	0.6
Ma et al. [73]	1.33	0.72	0.57

some variables, polynomial regression was used to quantitatively study the relationship between building density, building height, and the three optimization objectives, and the results are shown in Fig. 12. The three optimization objectives show a nonlinear relationship with the building height, PVG shows a nonlinear relationship with the building density, while AUHII and EUI show an approximately linear relationship with the building density. The correlation coefficient between building density and total EUI is -0.453 , indicating a weak negative correlation. As building density increases, total EUI decreases due to the high inter-shading effect and reduced solar heat gain.

The correlation coefficient between density and AUHII is -0.615 , suggesting a relatively strong correlation. This indicates that the urban heat island effect is mitigated with the increase building density, aligning with findings from existing studies. For example, Takkanon

[77] found that UHII is higher in medium-density areas with low height-to-width ratios compared to high-density areas with high ratios. The mutual shading effect and vegetation coverage in high-density neighborhoods can neutralize increased local temperature due to reduced permeability and ventilation.

Regarding photovoltaic generation, building density shows a strong positive correlation (0.552). Higher building density provides a large building surface area for PV installation, resulting in increased energy generation. The increased PV installation area outweighed the decreased PV generation due to mutual shading.

The relationship between building height and the three objectives exhibits different patterns. Building height has a strong correlation with AUHII (0.672) and PVG (0.820), but only a weak correlation with EUI (0.158). As the number of high-rise buildings increases, the inter-shading effect reduces available solar radiation on building surfaces, primarily influencing PVG. There is a quadratic nonlinear correlation between building height and PV generation. As the building height increases to a certain point (about 100 m), PV generation will initially

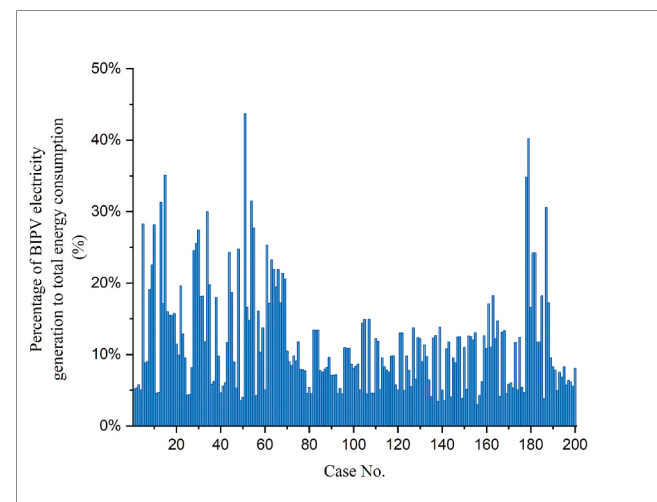


Fig. 11. The proportion of annual BIPV production to total annual energy consumption.

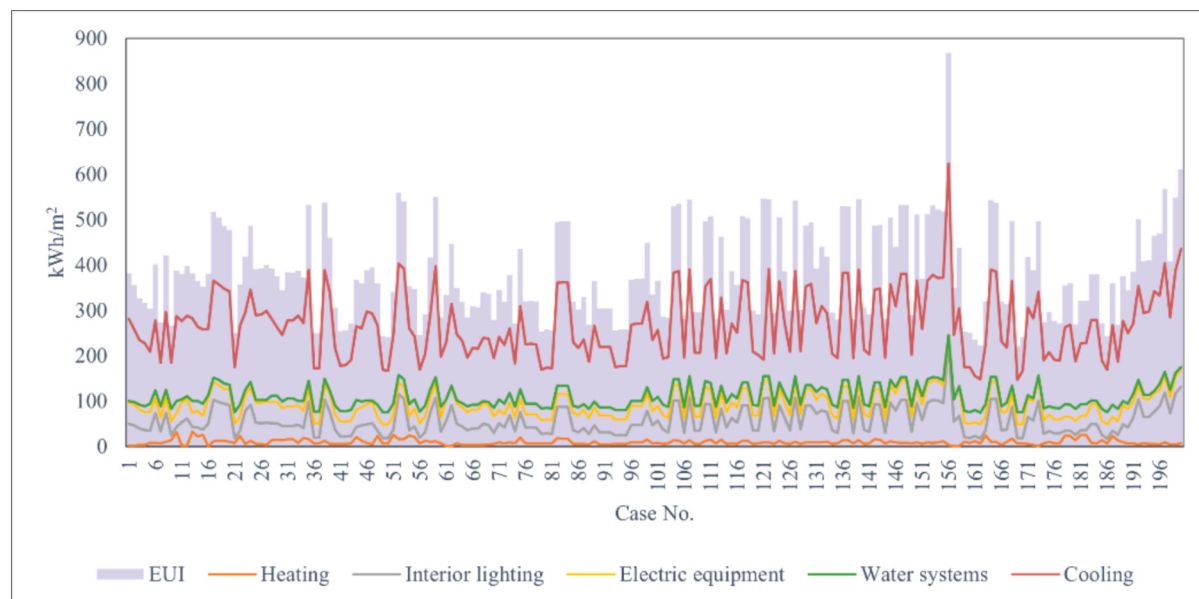


Fig. 10. Distribution characteristics of building energy consumption in different urban forms.

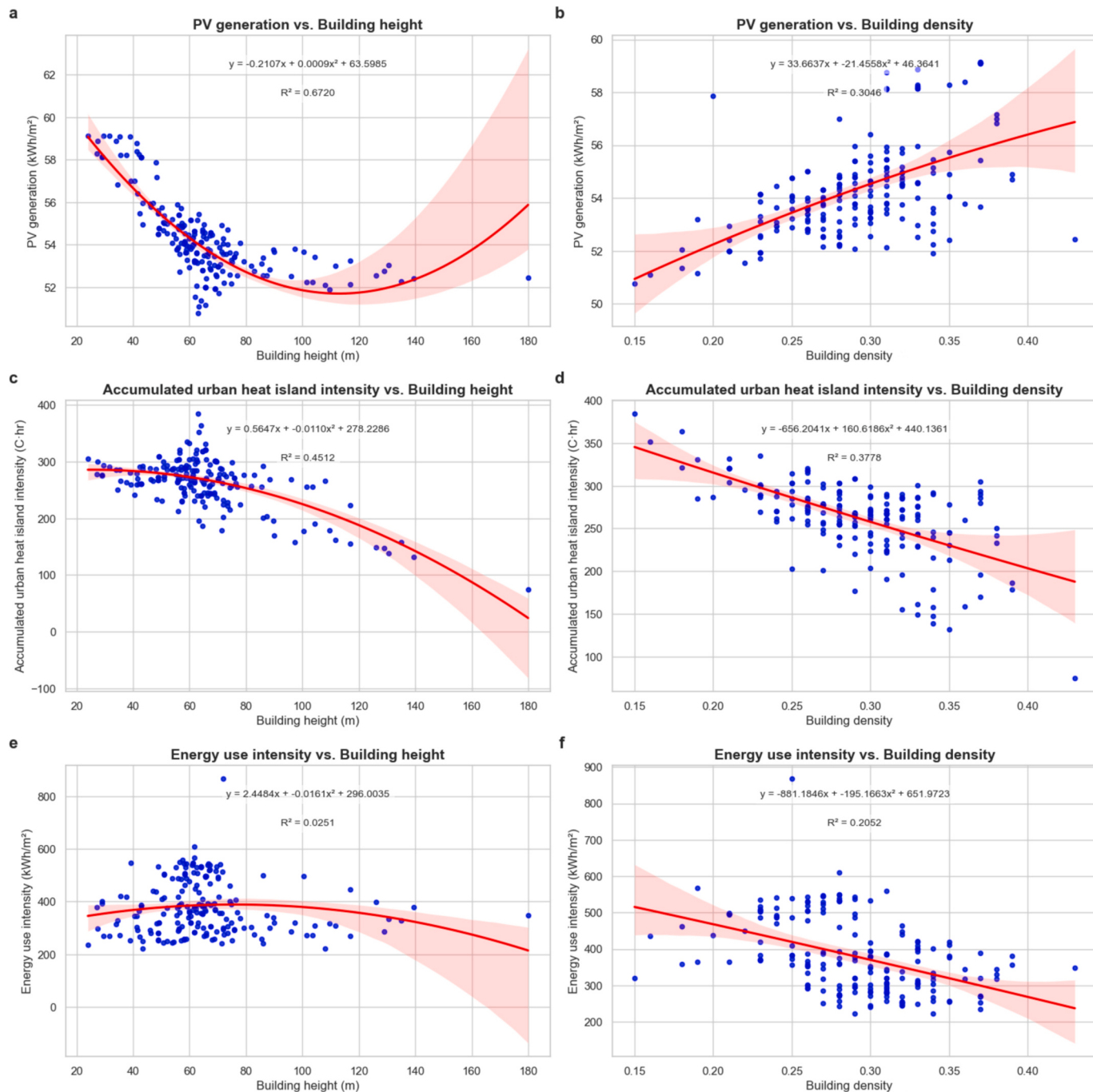


Fig. 12. Scatter plot of three optimization objectives and building density/building height. (The red area represents the 95 % confidence intervals). (For interpretation of the references to colour in this figure legend, the reader is referred to the web version of this article.)

decrease. However, as the building height increases further, PV generation may begin to increase again. When building height increase within a certain block design, the shading effect may outweigh the increased surface area for PV installation. The shading effect also mitigates the urban heat island intensity, and the channeling effect formed by surrounding high-rise buildings facilitate air circulation and heat dissipation, alleviating the urban heat island phenomenon. When the building height continues to increase, despite the existence of the shading effect, high-rise buildings can provide a larger surface area for installing photovoltaic panels, thereby increasing PV generation.

Xu et al. [78] found that block morphology influences office building energy consumption, demonstrating that building density (BD) and building height (BH) are negatively correlated with EUI. Similarly, Xie

et al. [79] showed the building density and average block height are negatively correlated with EUI and solar energy generation intensity (SEGI). The building height has a weak correlation with EUI and a strong correlation with SEGI, aligning with our results.

Table 6 presents the average values and standard deviations for three optimization objectives across different conditions as shown in Fig. 12. For PVG, the standard deviations are small for both the building height (54.27 ± 1.48 kWh/m²) and density (54.27 ± 1.00 kWh/m²), suggesting that PVG almost unaffected by their variations. The average AUHII is 263.75 °C·hr, with standard deviations of 28.68 for the building height and 26.24 for the building density, indicating a moderate sensitivity to these factors and a relatively wider distribution. EUI has an average of 379.69 kWh/m², with a small standard deviation of 16.16 for building

Table 6

Average values and standard deviation for three objectives under different conditions.

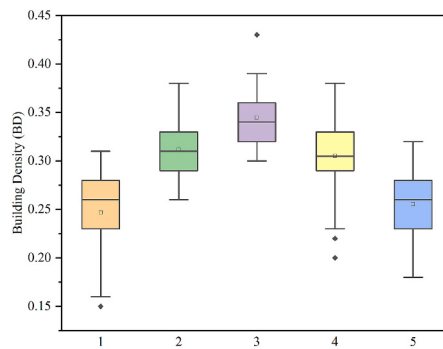
a	b	c	d	e	f
PVG vs Building height	PVG vs Building density	AUHII vs Building height	AUHII vs Building density	EUI vs Building height	EUI vs Building density
Avg	54.27	54.27	263.75	263.75	379.69
Std Dev	1.48	1.00	28.68	26.24	16.16
					46.18

height but a much larger value of 46.18 for the building density, indicating that EUI is more sensitive to density changes with a broader distribution. Thus, variations in the building density have a more pronounced effect on UHI and EUI, making it an important factor in the urban layout optimization.

3.2.2. Cluster analysis and performance optimization

The K-means clustering algorithm was employed to classify all solutions and extract representative parameters for research purposes. By comparing the clustering results for different values of k, it was found that setting k to 5 can effectively highlight morphological differences across clusters, while achieve similar morphological characteristics within the same cluster. The characteristics of the 5 clusters are presented in Fig. 13. Cluster 3 represents blocks with the highest median building density and building height, exhibiting a wide range of building heights and diverse architectural forms. For Cluster 2 and 4, the median values of building density and height are similar. However, they differ in terms of specific block forms such as the location of high-rise building and grass land. Buildings in Cluster 2 are more scattered, while Cluster 4 exhibits great variation in the building density. Additionally, blocks represented by Cluster 1 and Cluster 5 share similar characteristics, such as the single building type, low building density, and evenly distributed building height. However, Cluster 1 has a lower building density with a relatively larger variation range, whereas Cluster 5 includes outliers in building height. Table 7 displays the results of optimization objectives of corresponding clusters. Cluster 2 and 5 contain a larger solution number of 68 and 51, respectively. Cluster 1 and 4 comprise a moderate solution number of 27 and 36, respectively. Cluster 3 has the smallest number of 17.

Fig. 14 shows the distribution of clustered solutions in three objectives. Cluster 3 exhibits a generally low level of overall photovoltaic generation, while Clusters 2 and 4 demonstrate higher levels. Especially for Cluster 4, the overall range of PVG is between 53 and 58 kWh/m²/y, indicating a wide distribution range with a larger number of solutions achieving high power generation levels. For Cluster 1, the overall level of PVG is relatively poor, with not only a smaller median value but also a wider distribution of solutions in the low-level range. Cluster 5 shows an average level of PVG. Regarding AUHII, Cluster 3 performs the best, followed by Clusters 2, 4 and 5. Cluster 1 shows the worst performance,

**Fig. 13.** Distribution of building density and building height in different clusters (1–5).**Table 7**

Clustering results of optimization objectives.

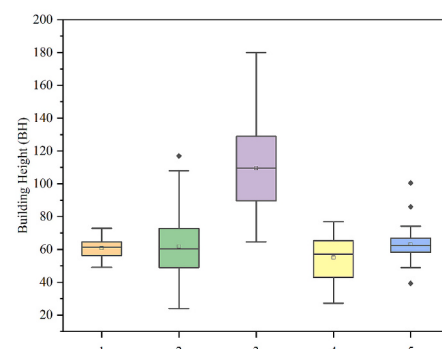
Cluster	Dataset	Cluster Centers		
		PVG (kWh/m ² /y)	AUHII (°C•hr)	EUI (kWh/m ² /y)
Cluster 1	27	53.246	313.2	361.35
Cluster 2	68	54.869	266.8	278.44
Cluster 3	17	53.198	164.8	344.32
Cluster 4	36	55.230	256.3	394.37
Cluster 5	51	53.712	272.9	516.25

and even more outliers. In terms of EUI, Cluster 2 demonstrates excellent performances, with the lowest building energy consumption level among different block designs, followed by Clusters 3, 1 and 4. Cluster 5 consumes the most energy and does not meet the energy-saving goals. In summary, when considering the three optimization objectives simultaneously, Clusters 2 and 4 display relatively balanced performance, Cluster 3 shows relatively poor performance, while Clusters 1 and 5 exhibit the worst performance.

Fig. 15 depicts the correlation between building density, building height, and the respective iMOO score values across all scenarios. It is evident that when the building density ranges from 0.3 to 0.4 and the building height falls between 20 and 50 m, all three objectives can be optimized. Moreover, the scheme that possesses the lowest iMOO score can be eventually identified as the optimum solution.

Table 8 shows the top 15 optimal solutions in terms of the iMOO score and corresponding objective values. From the generated building design scenarios, the minimum iMOO score derived from normalized PVG, AUHII, and EUI values, is 0.1444, while holds a building density of 0.37 and building height of 39 m. And the urban block can achieve the optimal integrated performance with PVG, AUHII, and EUI as 59.08 kWh/m², 280.1 °C•hr, and 253.38 kWh/m² respectively.

The findings above demonstrate that the urban block form has a significant impact on building energy consumption, solar energy potential, and urban microclimate. There is also a possibility to achieve a tradeoff between the three objectives. For urban designers, selecting appropriate urban morphology can maximize the solar energy utilization in neighborhoods while minimizing building energy consumption and urban heat island intensity. This is particularly crucial for building energy conservation, renewable energy utilization and climate change mitigation. By integrating quantitative analysis with intuitive multi-objective optimization results, this paper contributes to a deeper understanding of the relationship and mechanisms between urban morphology, microclimate and energy performance. Furthermore, the research findings offer important references and support for urban development, especially in areas with limited land, high-rise buildings and similar climates.



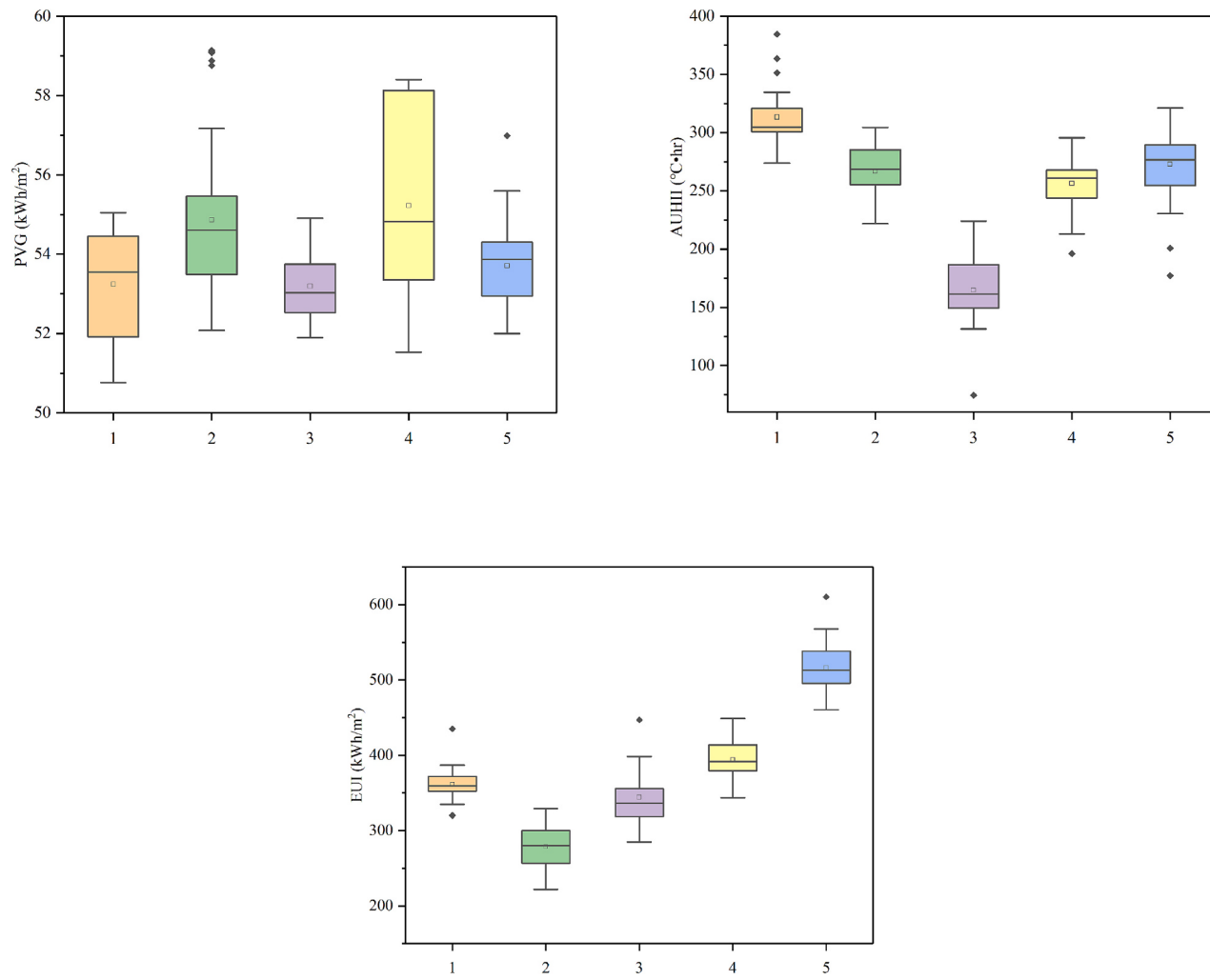


Fig. 14. Results of PVG, AUHII, EUI in five clusters.

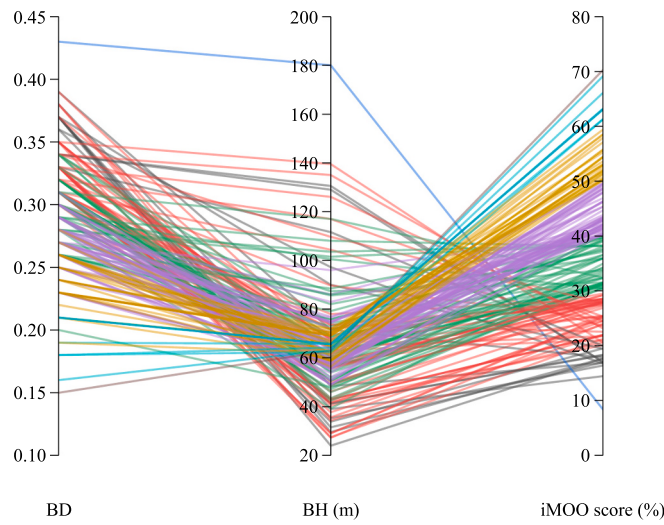


Fig. 15. The parallel coordinate diagram of BD, BH, and iMOO score.

Table 8
Building design scenarios.

Building density	Building height	PVG	AUHII	EUI	iMOO score	Cluster
-	m	kWh/m ²	°C·hr	kWh/m ²	-	-
0.37	39	59.08	280.1	253.38	0.1444	2
0.37	24	59.14	304.4	235.23	0.1767	2
0.37	35.3	59.09	285.6	271.355	0.1638	2
0.37	31.5	59.11	290.2	268.632	0.1700	2
0.37	29.6	59.11	293.5	269.86	0.1767	2
0.31	41.4	58.76	279.3	303.047	0.1826	2
0.33	33.9	58.88	285.5	313.786	0.1950	2
0.33	27.4	58.88	300.1	296.055	0.2121	2
0.36	41.2	58.40	259.6	345.05	0.1836	4
0.38	48.4	57.17	232.7	318.31	0.1687	2
0.33	42	58.27	260.2	365.64	0.2010	4
0.38	40.4	56.99	241.5	343.754	0.2058	4
0.31	42.9	58.13	261	385.242	0.2189	4
0.31	42.9	58.13	261	385.76	0.2190	4
0.31	42.9	58.13	261	386.92	0.2196	4

3.3. Discussion

The statistical analysis and optimization framework proposed in this study can actually be applied to other regions, providing valuable support for urban design and contributing to the goal of sustainable and energy-efficient urban development. Furthermore, the strong correlation identified with building energy consumption and solar PV potential can be observed not only in other cities with similar climates, such as Shenzhen [80] and Adelaide [81], but also in cities with diverse climates such as Nanjing [82], Wuhan [83], Vienna [84], and even Harbin [85], as shown in Table 9. The building height and building density are among the most important factors influencing urban morphology, while the urban heat island effect is highly dependent on local climates.

Microclimate modelling with UWG maintains similar accuracy only for homogeneous cities within the same climate zone. Significant differences in AUHII may occur in highly heterogeneous urban areas [86]. Therefore, the results of this study are applicable only to regions with climate conditions similar to those of Hong Kong and must be validated before being applied to regions with substantially different climates.

In the study of urban microclimate and BIPV, although temperature is a key factor for individual PV panels, it is not the most important factor affecting overall PV power generation efficiency in neighborhood / urban-scale applications. The overall PV power generation efficiency is more greatly influenced by the aspect ratio and canyon orientation [87,88]. Wei et al. [89] further demonstrated that urban canyons with PV modules exhibit little change in air temperature compared to those without PV, given the complex interactions in urban microclimates. Therefore, the influence of canyon temperature on the efficiency of photovoltaic panels is not considered in this study. However, as above studies adopted simplified physical models and smaller-scale simulations when modelling the interactions between BIPV and urban energy performance. Large-scale applications of photovoltaic panels may alter the temperature of building envelopes and peripheral thermal environment, thereby affecting PV power generation [90].

Additionally, the Hong Kong government introduced the Feed-in Tariff (FiT) Scheme and Renewable Energy Certificates (RE Certificates) Scheme in 2017. The FiT scheme provides a fixed purchase price for photovoltaic (PV) electricity, ensuring a return on investment, while the RE Certificates scheme allows the sale of environmental benefits to further offset installation and operational costs. Zhang et al. [91,92] highlight the role of FiT and REC schemes in achieving grid parity, ensuring economic profitability for PV system installers. Therefore, the economic factor is not a major constraint for BIPV deployment in Hong Kong considering the necessity to achieve the carbon neutrality target

before 2050, while the technical and environmental impacts become the focus of this research.

3.4. Limitation and future work

This study has several limitations that should be addressed in future research: (1) The absolute correlation level may vary in different climates, and the developed framework will be applied to urban environments in different climate zones, such as temperate, polar, and tropical cities. The model's applicability can then be validated through cross-climate assessment. (2) In the sensitivity analysis section, this paper focuses on the influence of urban characteristics and vegetation parameters on microclimate modelling results. Future studies can integrate traffic data, vehicle types, and travel patterns, traffic heat emission simulation tools (such as the heat source module in ENVI-MET) to assess their impact on urban microclimates, especially in high-traffic areas, for a more comprehensive microclimate modelling. (3) To more accurately assess the performance of photovoltaic systems in urban environments, future research should focus on developing and utilizing actual weather data, and consider additional microclimate factors, such as temperature and wind speed, for a more comprehensive evaluation. This will involve modification of existing models and experimental validations to ensure the accuracy and reliability of simulation results. (4) To comprehensively evaluate the sustainability of BIPV, future studies should include a multidimensional analysis in lifecycle assessment (LCA) by integrating technical, environmental, and economic factors. LCA tools can be employed to simulate BIPV's resource consumption and emissions throughout production, operation, maintenance, and disposal, incorporating economic costs and environmental impact factors. This integrated assessment will help in understanding the long-term feasibility of BIPV in different countries and regions (with and without subsidies) and serve as a foundation for policy and investment decisions.

4. Conclusion

This paper establishes a framework coupling feature extraction for microclimate simulation, parametric modelling and design optimization for integrated urban performance evaluation as well as post-processing statistical analysis. The optimal urban block design is explored by simultaneously considering the building energy efficiency, solar energy utilization and urban heat island mitigation. The main findings can be summarized as follows:

(1) The developed sensitivity analysis approach coupling the High Dimensional Model Representation (HDMR) and Urban Weather

Table 9

Effects of BD and BH on energy consumption and solar PV potential in different climate zones.

Country	Climate zones	Results
Shenzhen [80]	Cwa	Building density and building height have a significant impact on solar potential.
Adelaide [81]	Csa	Two types of low-density, low-rise neighborhoods in Adelaide (i.e., non-uniform-sized and uniform-sized) have the highest solar potential.
Nanjing [82]	Cfa	The site coverage ratio and average building height have the strongest correlation with annual solar radiation.
Wuhan [83]	Cfa	Tower buildings with low heights (9–21 m) and low densities (0.21–0.34) have higher potential solar power generation.
Vienna [84]	Cfb	Site coverage has a decisive impact on solar potential and energy requirement.
Harbin [85]	Dwa	Building site coverage and building height have a strong relationship with energy consumption.

Notes: The site coverage ratio, site coverage, building site cover mentioned above have the same definition with building density in this paper.

Generator can perform robust feature extraction to determine the most important urban block design parameters. The sensitivity analysis results reveal that building density and building height are the most influential parameters. The reliability of sensitivity indices is also validated by bootstrapping.

(2) The effect of building height on the three target values is non-linear, while the impact of building density on photovoltaic generation (PVG) is non-linear, and the impact on energy use intensity (EUI) and accumulated urban heat island intensity (AUHII) is approximately linear. Polynomial regression analysis results indicate that building density has a weak negative correlation with EUI and a strong negative correlation with AUHII. A High-density neighborhood can still mitigate the urban heat island effect by adjusting the vegetation coverage and mutual shading effect between buildings. However, the relationship between building height and three objectives shows a different pattern, it has a strong positive correlation with AUHII and PVG, while weak correlation with EUI. Within a certain range, as the number of high-rise buildings increases, the inter-shading effect has negative effect on the available solar radiation on building surfaces. In addition, building density has a positive correlation with PVG but a negative correlation with AUHII and EUI. Considering the reduction in PVG due to mutual shading, higher building density allows for a wider range of PV installations, resulting in higher power generation.

(3) K-means cluster analyses of all simulation results yield five clusters, with Cluster 2 containing the highest number of results. Each cluster demonstrates different performance advantages for different optimization objectives. Cluster 3 performs the best in terms of AUHII, while Cluster 2 performs better overall for EUI. However, for PVG, Cluster 2 and 4 exhibit better performance. Based on comprehensive evaluation of different urban block design objectives and iMOO score, when the building density is between 0.3 and 0.4 and the building height is between 20 and 50 m, the overall performance of the block is the best. Meanwhile, the EUI, PVG, and AUHII of the optimal solution is

determined as 253.38 kWh/m², 59.08 kWh/m², and 280.1 °C•hr respectively when the building density is 0.37 and the building height is 39 m.

By combining quantitative feature analysis with intuitive multi-objective optimization results, this paper contributes to a deeper understanding of the relationship and mechanism between the urban morphology, microclimate, building energy consumption and solar PV power potential. Furthermore, the research results emphasize the importance of considering building density, building height and their interactions to reduce overall urban energy demand and regulate local climate, providing a valuable reference for future urban block designs to reduce the overall urban energy demand and regulate the local climate.

CRediT authorship contribution statement

Chenhang Bian: Writing – review & editing, Writing – original draft, Visualization, Validation, Methodology, Investigation, Formal analysis.
Ka Lung Cheung: Visualization, Methodology. **Xi Chen:** Writing – review & editing, Supervision, Funding acquisition, Conceptualization.
Chi Chung Lee: Supervision, Funding acquisition.

Declaration of competing interest

The authors declare that they have no known competing financial interests or personal relationships that could have appeared to influence the work reported in this paper.

Acknowledgement

This work was sponsored by the CUHK Direct Grant for Research No. 4055168 and the Research Grants Council of the Hong Kong Special Administrative Region, China (UGC/FDS16/E04/21 and UGC/FDS16/E10/22).

Appendix A. Dry-bulb temperature, wind speed and solar radiation in a typical meteorological year in Hong Kong

The annual dry bulb temperature distribution is shown in Fig. A1. The hottest month is July, with an average temperature of 28.8 °C, while the coldest month is January, with an average temperature of 16.1 °C. Therefore, the building cooling demand is high in this region. Additionally, based on the wind rose diagram in Fig. A2, it can be observed that the dominant wind directions in summer are from the east and west, with an average wind speed of 3.12 m/s. In winter, the dominant wind direction is from the east and northeast, with an average wind speed of 3.07 m/s.

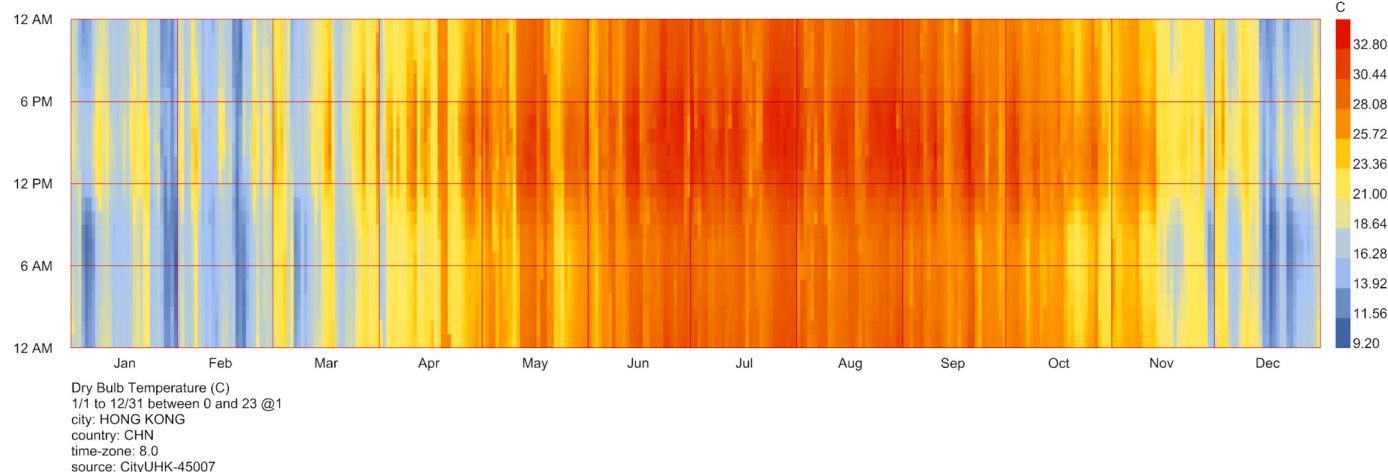


Fig. A1. Dry bulb temperature of TMY.

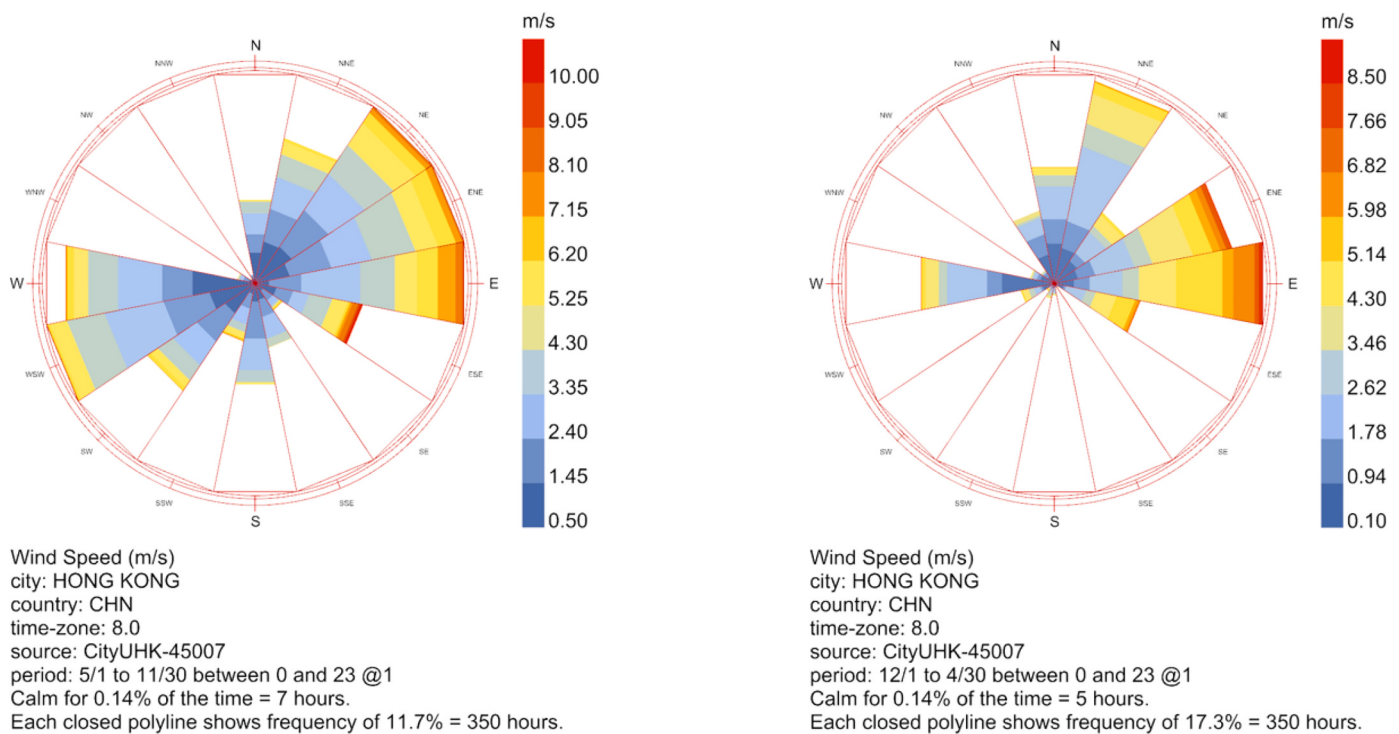


Fig. A2. Wind rose plots for the summer and winter period of Hong Kong. (For interpretation of the references to colour in this figure legend, the reader is referred to the web version of this article.)

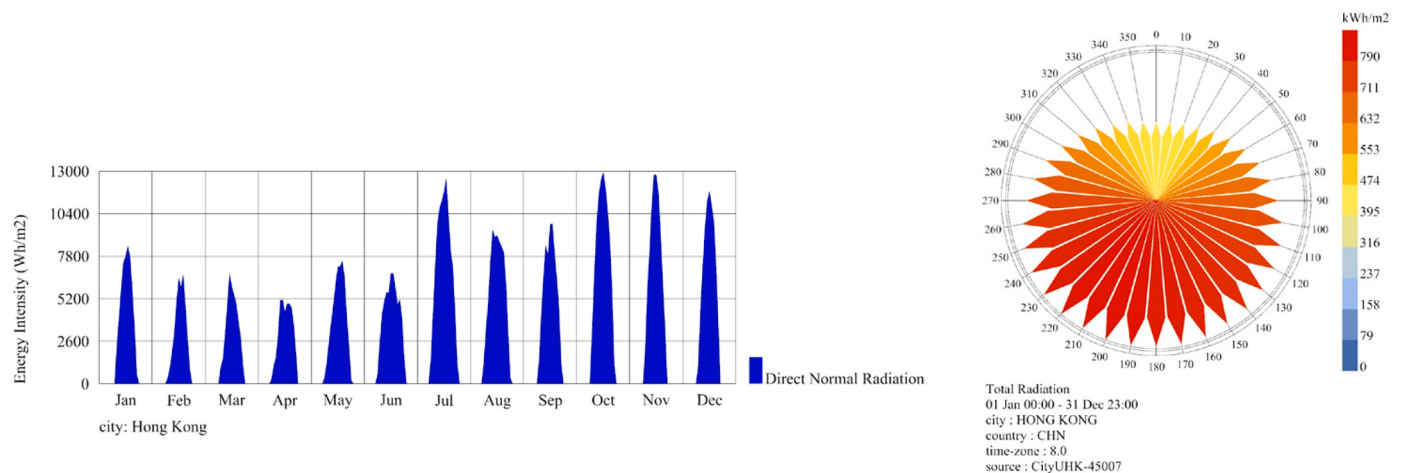


Fig. A3. Direct normal solar radiation and radiation rose. (For interpretation of the references to colour in this figure legend, the reader is referred to the web version of this article.)

Solar energy is one of the primary renewable energy sources, and its utilization efficiency is highly correlated with the region and season [93]. Hong Kong, located in the southern part of China, experiences relatively high solar radiation compared to most regions in China. Fig. A3 shows its distribution of solar radiation across different months in a typical year. The summer months have the highest solar radiation, while the winter months have relatively less. Overall, the distribution is relatively balanced, indicating a high potential for solar energy utilization. Buildings facing south receive the highest amount of solar heat.

Appendix B. Detailed simulation process and parameter settings in Grasshopper

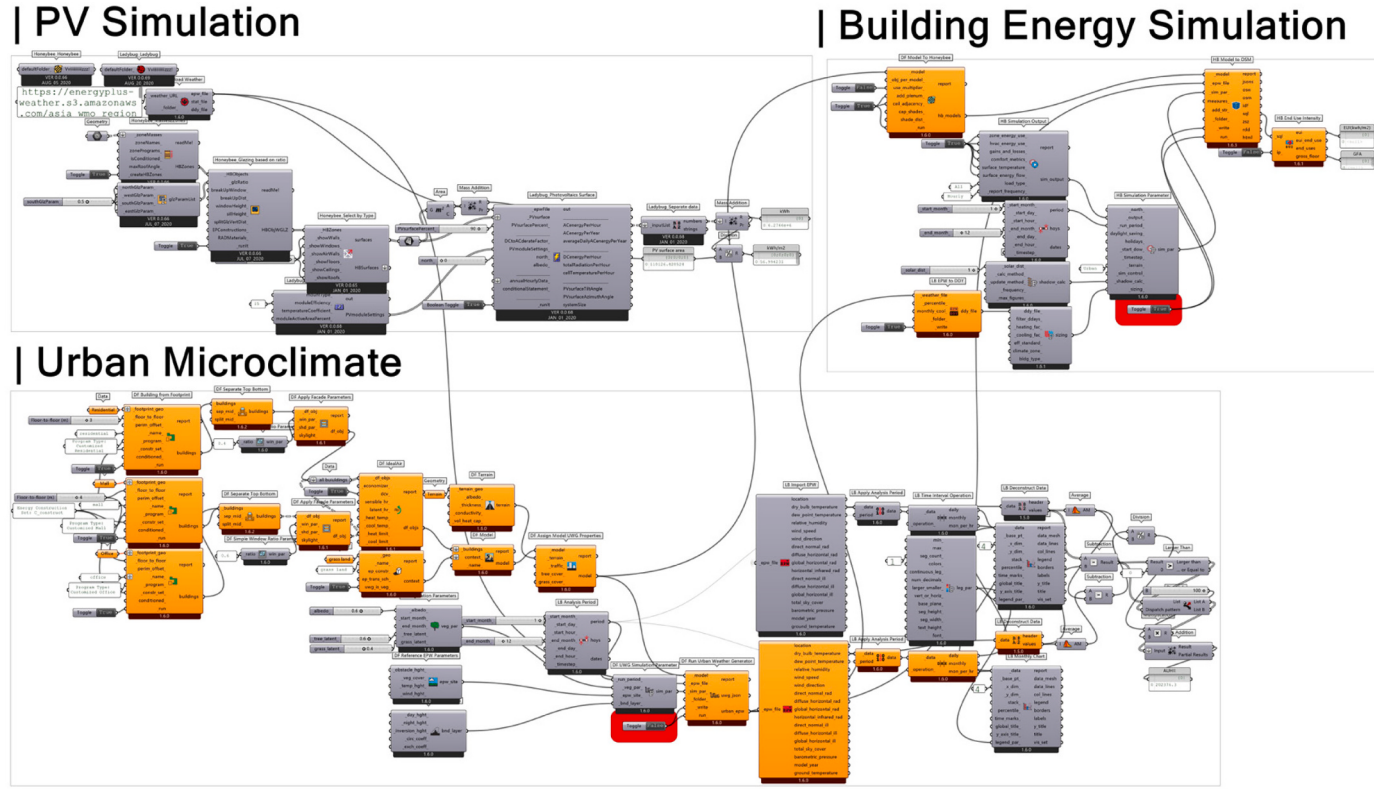


Fig. B1. Detailed model generation and simulation process in grasshopper.

Table B1

Parameter setting buildings and integrated PV systems.

Parameters	Settings		
Building typology			
U-value of external wall	Residential 0.678 W/ (m ² • k)	Office	Mall
U-value of roof	0.52 W/ (m ² • k)		
U-value of window	5.76 W/ (m ² • k)		
Building constructions			
Floor-to-floor height	3 m	4 m	
Window-to-wall ratio	0.4	0.6	
Program			
People density	0.028 people/ m ²	0.077 people/ m ²	0.1 people/ m ²
Lighting power density	4 W/m ²	15 W/m ²	23 W/m ²
Equipment power density	5 W/m ²	10 W/m ²	4.3 W/m ²
PV			
Cooling setpoint	24 °C		
Infiltration intensity	0.001133 m ³ /s/m ²		
PV module	c-Si		
System efficiency	15 %		
Module active area percent	90 %		
Simulation settings	Period 8760 h		
	Vegetation albedo 0.6		

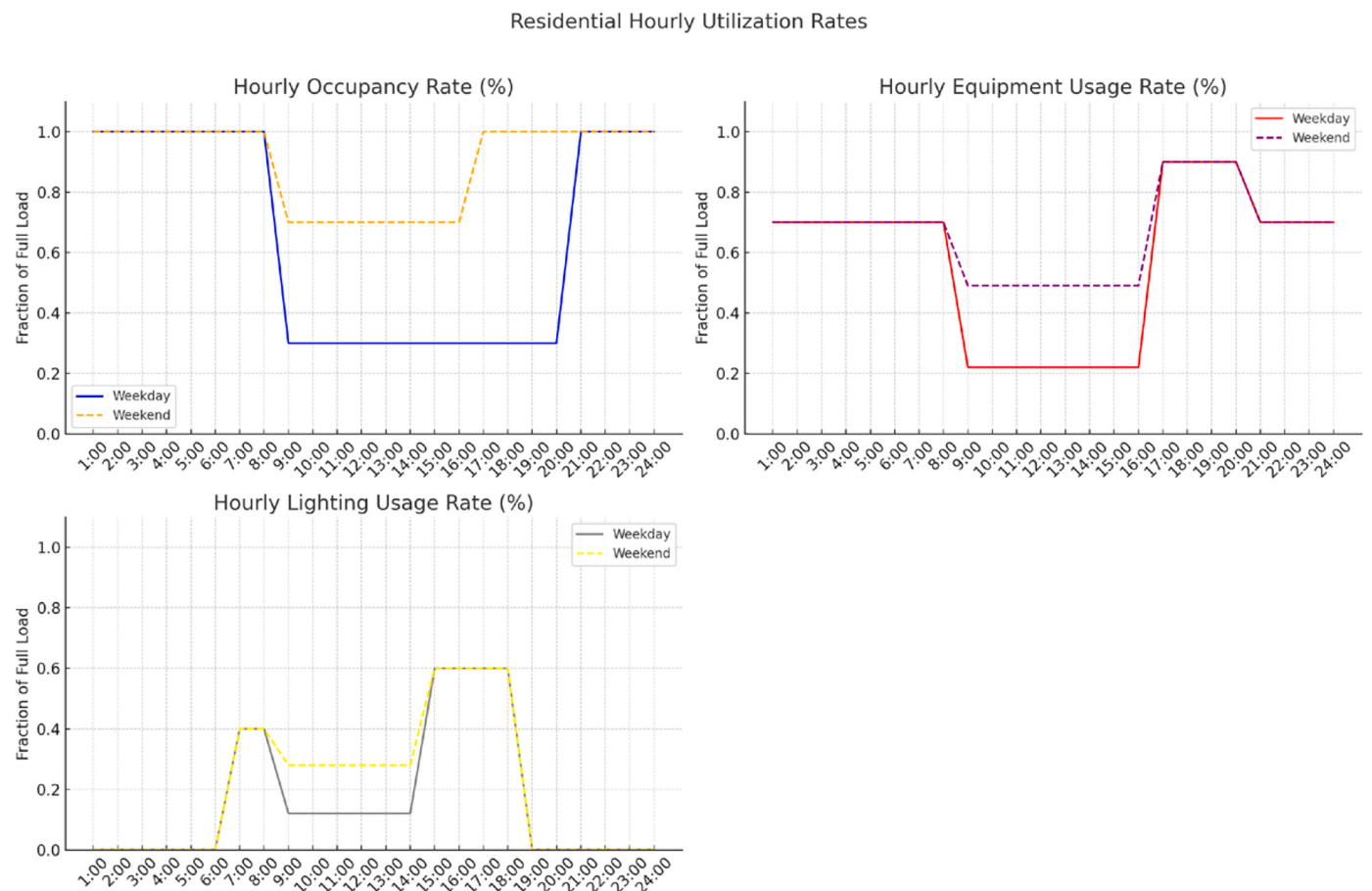


Fig. B2. Schedule setting of residential building [94].

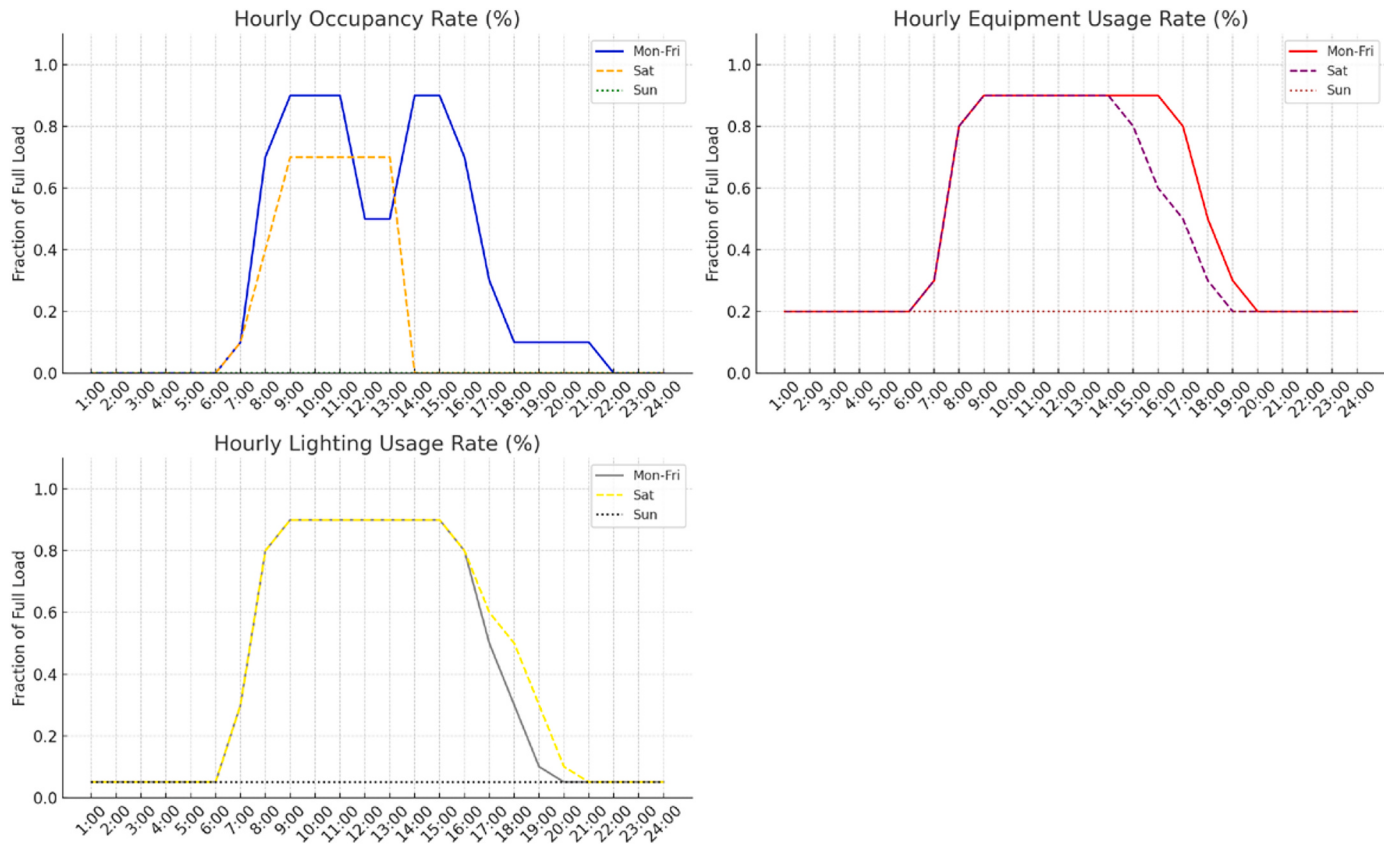


Fig. B3. Schedule setting of office and mall building [95].

Data availability

Data will be made available on request.

References

- [1] Cdb P. Global status report for buildings and construction 2022. 2022.
- [2] Dong H, Zhang L. Transition towards carbon neutrality: forecasting Hong Kong's buildings carbon footprint by 2050 using a machine learning approach. Sustain Prod Consum 2023;35:633–42. <https://doi.org/10.1016/j.spc.2022.12.014>.
- [3] Arbazdeh V, Frank R. Creating a renewable energy-powered energy system: extreme scenarios and novel solutions for large-scale renewable power integration. Appl Energy 2024;374:124088. <https://doi.org/10.1016/j.apenergy.2024.124088>.
- [4] Tian X, Zhang H, Liu L, Huang J, Liu L, Liu J. Establishment of LCZ-based urban building energy consumption dataset in hot and humid subtropical regions through a bottom-up method. Appl Energy 2024;368:123491. <https://doi.org/10.1016/j.apenergy.2024.123491>.
- [5] Shang Y, Sang S, Tiwari AK, Khan S, Zhao X. Impacts of renewable energy on climate risk: a global perspective for energy transition in a climate adaptation framework. Appl Energy 2024;362:122994. <https://doi.org/10.1016/j.apenergy.2024.122994>.
- [6] Li X, Zhou Y, Yu S, Jia G, Li H, Li W. Urban heat island impacts on building energy consumption: a review of approaches and findings. Energy 2019;174:407–19. <https://doi.org/10.1016/j.energy.2019.02.183>.
- [7] Kamal A, Mahfouz A, Sezer N, Hassan IG, Wang LL, Rahman MA. Investigation of urban heat island and climate change and their combined impact on building cooling demand in the hot and humid climate of Qatar. Urban Clim 2023;52: 101704. <https://doi.org/10.1016/j.uclim.2023.101704>.
- [8] Zhang Y, Teoh BK, Zhang L. Multi-objective optimization for energy-efficient building design considering urban heat island effects. Appl Energy 2024;376: 124117. <https://doi.org/10.1016/j.apenergy.2024.124117>.
- [9] Saleh A, Saleh N, Ali O, Hasan R, Ahmed O, Alias A, et al. Green building techniques: under the umbrella of the climate framework agreement. Babylon J Mach Learn 2024;2024:1–14. <https://doi.org/10.58496/BJML/2024/001>.
- [10] Bueno B, Norford L, Hidalgo J, Pigeon G. The urban weather generator. J Build Perform Simul 2013;6:269–81. <https://doi.org/10.1080/19401493.2012.718797>.
- [11] Aiko N. Urban weather generator user interface development : Towards a usable tool for integrating urban heat island effect within urban design process. 2015. <https://dspace.mit.edu/handle/1721.1/99251> (accessed December 18, 2023).
- [12] Nakano A, Bueno B, Norford L, Reinhart C. Urban weather generator – a novel workflow for integrating urban heat island effect within urban design process. 2015. <https://doi.org/10.26868/25222708.2015.2909>.
- [13] Salvati A, Monti P, Coch Roura H, Cecere C. Climatic performance of urban textures analysis tools for a mediterranean urban context. Energ Build 2019;185: 162–79. <https://doi.org/10.1016/j.enbuild.2018.12.024>.
- [14] Yang JH, Joseph H. The curious case of urban heat island : A systems analysis. Thesis. Massachusetts Institute of Technology; 2016.
- [15] Boccalatte A, Fossa M, Gaillard L, Menezo C. Microclimate and urban morphology effects on building energy demand in different European cities. Energ Build 2020; 224:110129. <https://doi.org/10.1016/j.enbuild.2020.110129>.
- [16] Shen P, Liu J, Wang M. Fast generation of microclimate weather data for building simulation under heat island using map capturing and clustering technique. Sustain Cities Soc 2021;71:102954. <https://doi.org/10.1016/j.scs.2021.102954>.
- [17] Xu G, Zhao H, Li J, Shi Y, Feng X, Zhang Y. Multivariate thermal environment data extraction and evaluation: a neighborhood scale case in Guangzhou. China Build Environ 2023;234:110190. <https://doi.org/10.1016/j.buildenv.2023.110190>.
- [18] Reitberger R, Palm N, Palm H, Lang W. Urban systems exploration: a generic process for multi-objective urban planning to support decision making in early design phases. Build Environ 2024;254:111360. <https://doi.org/10.1016/j.buildenv.2024.111360>.
- [19] Nakano A, Bueno B, Norford L, Reinhart C. Urban weather generator – a novel workflow for integrating urban heat island effect within urban design process. 2015. <https://doi.org/10.26868/25222708.2015.2909>.
- [20] Xu X, Liu Y, Wang W, Xu N, Liu K, Yu G. Urban layout optimization based on genetic algorithm for microclimate performance in the cold region of China. Appl Sci 2019;9:4747. <https://doi.org/10.3390/app9224747>.
- [21] Aydin EE, Ortner FP, Peng S, Yenardi A, Chen Z, Tay JZ. Climate-responsive urban planning through generative models: sensitivity analysis of urban planning and design parameters for urban heat island in Singapore's residential settlements. Sustain Cities Soc 2024;114:105779. <https://doi.org/10.1016/j.scs.2024.105779>.
- [22] Litardo J, Palme M, Borbor-Cordova M, Caiza R, Macias J, Hidalgo-Leon R, et al. Urban heat island intensity and buildings' energy needs in Duran, Ecuador: simulation studies and proposal of mitigation strategies. Sustain Cities Soc 2020; 62:102387. <https://doi.org/10.1016/j.scs.2020.102387>.

- [23] Liu J, She X, Wang J. Comprehensive optimization of urban building cluster morphology based on microclimate: a two-level optimization approach. *Sustain Cities Soc* 2024;100:105005. <https://doi.org/10.1016/j.scs.2023.105005>.
- [24] Sezer N, Yoonus H, Zhan D, Wang L, Leon, Hassan IG, et al. Urban microclimate and building energy models: a review of the latest progress in coupling strategies. *Renew Sust Energ Rev* 2023;184:113577. <https://doi.org/10.1016/j.rser.2023.113577>.
- [25] Sun H, Heng CK, Tay SER, Chen T, Reindl T. Comprehensive feasibility assessment of building integrated photovoltaics (BIPV) on building surfaces in high-density urban environments. *Sol Energy* 2021;225:734–46. <https://doi.org/10.1016/j.solener.2021.07.060>.
- [26] Liao X, Zhu R, Wong MS, Heo J, Chan PW, Kwok CYT. Fast and accurate estimation of solar irradiation on building rooftops in Hong Kong: a machine learning-based parameterization approach. *Renew Energy* 2023;216:119034. <https://doi.org/10.1016/j.renene.2023.119034>.
- [27] Reffat RM, Ezzat R. Impacts of design configurations and movements of PV attached to building facades on increasing generated renewable energy. *Sol Energy* 2023;252:50–71. <https://doi.org/10.1016/j.solener.2023.01.040>.
- [28] Liu R, Liu Z, Xiong W, Zhang L, Zhao C, Yin Y. Performance simulation and optimization of building façade photovoltaic systems under different urban building layouts. *Energy* 2023;129708. <https://doi.org/10.1016/j.energy.2023.129708>.
- [29] Liao X, Zhu R, Wong MS, Heo J, Chan PW, Kwok CYT. Fast and accurate estimation of solar irradiation on building rooftops in Hong Kong: a machine learning-based parameterization approach. *Renew Energy* 2023;216:119034. <https://doi.org/10.1016/j.renene.2023.119034>.
- [30] Elhabodi TS, Yang S, Parker J, Khattak S, He B-J, Attia S. A review on BIPV-induced temperature effects on urban heat islands. *Urban Clim* 2023;50:101592. <https://doi.org/10.1016/j.ulclim.2023.101592>.
- [31] Wu H, Deng F, Tan H. Research on parametric design method of solar photovoltaic utilization potential of nearly zero-energy high-rise residential building based on genetic algorithm. *J Clean Prod* 2022;368:133169. <https://doi.org/10.1016/j.jclepro.2022.133169>.
- [32] Liu K, Xu X, Zhang R, Kong L, Wang W, Deng W. Impact of urban form on building energy consumption and solar energy potential: a case study of residential blocks in Jianhu, China. *Energy Build* 2023;280:112727. <https://doi.org/10.1016/j.enbuild.2022.112727>.
- [33] Li Z, Ma J, Jiang F, Zhang S, Tan Y. Assessing the impacts of urban morphological factors on urban building energy modeling based on spatial proximity analysis and explainable machine learning. *J Build Eng* 2024;85:108675. <https://doi.org/10.1016/j.jobe.2024.108675>.
- [34] Hadavi M, Pasdarshahi H. Investigating effects of urban configuration and density on urban climate and building systems energy consumption. *J Build Eng* 2021;44:102710. <https://doi.org/10.1016/j.jobe.2021.102710>.
- [35] Wu H, Zhang T. Multi-objective optimization of energy, visual, and thermal performance for building envelopes in China's hot summer and cold winter climate zone. *J Build Eng* 2022;59:105034. <https://doi.org/10.1016/j.jobe.2022.105034>.
- [36] Tian J, Ooka R. Evaluation of solar energy potential for residential buildings in urban environments based on a parametric approach. *Sustain Cities Soc* 2024;106:105350. <https://doi.org/10.1016/j.scs.2024.105350>.
- [37] Wang W, Liu K, Zhang M, Shen Y, Jing R, Xu X. From simulation to data-driven approach: a framework of integrating urban morphology to low-energy urban design. *Renew Energy* 2021;179:2016–35. <https://doi.org/10.1016/j.renene.2021.08.024>.
- [38] Shao J, Pan C, Ji X. The functional research of the road guide for the high density city —taking hong kong for example. 2015.
- [39] Home | ashrae.org n.d. <https://www.ashrae.org/> (accessed December 25, 2023).
- [40] Chan ALS, Chow TT, Fong SKF, Lin JZ. Generation of a typical meteorological year for Hong Kong. *Energy Convers Manag* 2006;47:87–96. <https://doi.org/10.1016/j.enconman.2005.02.010>.
- [41] Cui L, Liu Z, Zhao X. Moment-independent importance measure of basic random variable and its probability density evolution solution. *Sci China Technol Sci* 2010;53:1138–45. <https://doi.org/10.1007/s11431-009-0386-8>.
- [42] Douglas-Smith D, Iwanaga T, Croke BFW, Jakeman AJ. Certain trends in uncertainty and sensitivity analysis: An overview of software tools and techniques. *Environ Model Softw* 2020;124:104588. <https://doi.org/10.1016/j.envsoft.2019.104588>.
- [43] Pianosi F, Beven K, Freer J, Hall JW, Rougier J, Stephenson DB, et al. Sensitivity analysis of environmental models: a systematic review with practical workflow. *Environ Model Softw* 2016;79:214–32. <https://doi.org/10.1016/j.envsoft.2016.02.008>.
- [44] Razavi S, Sheikholeslami R, Gupta HV, Haghnegahdar A. Vars-tool: a toolbox for comprehensive, efficient, and robust sensitivity and uncertainty analysis. *Environ Model Softw* 2019;112:95–107. <https://doi.org/10.1016/j.envsoft.2018.10.005>.
- [45] Herman J, Usher W. SALib: An open-source python library for sensitivity analysis. *J Open Source Softw* 2017;2:97. <https://doi.org/10.21105/joss.00097>.
- [46] Iwanaga T, Usher W, Herman J. Toward SALib 2.0: advancing the accessibility and interpretability of global sensitivity analyses. *Socio-Environ Syst Model* 2022;4:18155. <https://doi.org/10.18174/sesmo.18155>.
- [47] Basics — SALib's documentation. 2024 (accessed January 29, 2024), https://salib.readthedocs.io/en/latest/user_guide/basics.html.
- [48] Kwakkel JH. The exploratory modeling workbench: An open source toolkit for exploratory modeling, scenario discovery, and (multi-objective) robust decision making. *Environ Model Softw* 2017;96:239–50. <https://doi.org/10.1016/j.envsoft.2017.06.054>.
- [49] Saltelli A, Annoni P, Azzini I, Campolongo F, Ratto M, Tarantola S. Variance based sensitivity analysis of model output. Design and estimator for the total sensitivity index. *Comput Phys Commun* 2010;181:259–70. <https://doi.org/10.1016/j.cpc.2009.09.018>.
- [50] Morris MD. Factorial sampling plans for preliminary computational experiments. *Technometrics* 1991;33:161–74. <https://doi.org/10.1080/00401706.1991.10484804>.
- [51] Cukier RI, Fortuin CM, Shuler KE, Petschek AG, Schaibly JH. Study of the sensitivity of coupled reaction systems to uncertainties in rate coefficients. I Theory. *J Chem Phys* 2003;59:3873–8. <https://doi.org/10.1063/1.1680571>.
- [52] Li G, Rabitz H, Yelvington PE, Oluwole OO, Bacon F, Kolb CE, et al. Global sensitivity analysis for systems with independent and/or correlated inputs. *ACS Publ* 2010. <https://doi.org/10.1021/jp9096919>.
- [53] Rabitz H, Aliş ÖF. General foundations of high-dimensional model representations. *J Math Chem* 1999;25:197–233. <https://doi.org/10.1023/A:1019188517934>.
- [54] Planning department - land utilization in Hong Kong. 2023 (accessed August 1, 2024). https://www.pland.gov.hk/pland_en/info/ser/serve/open_data/landu/.
- [55] Block types | hong kong housing authority and housing department. 2023 (accessed August 1, 2024), <https://www.housingauthority.gov.hk/en/about-us/photos-and-videos/photo-albums/block-types/index.html>.
- [56] Liu S, Kwok Y-T, Lau K, Ng E. Applicability of different extreme weather datasets for assessing indoor overheating risks of residential buildings in a subtropical high-density city. *Build Environ* 2021;194:107711. <https://doi.org/10.1016/j.buildenv.2021.107711>.
- [57] Dai HK, Shi Y, Chen C. Developing a deep neural network model for predicting ventilation rates in public housing buildings in Hong Kong. *Energ Build* 2024;307:113993. <https://doi.org/10.1016/j.enbuild.2024.113993>.
- [58] Cui Y, Yan D, Hong T, Ma J. Temporal and spatial characteristics of the urban heat island in Beijing and the impact on building design and energy performance. *Energy* 2017;130:286–97. <https://doi.org/10.1016/j.energy.2017.04.053>.
- [59] Crawley DB, Lawrie LK, Winkelmann FC, Buhl WF, Huang YJ, Pedersen CO, et al. EnergyPlus: creating a new-generation building energy simulation program. *Energ Build* 2001;33:319–31. [https://doi.org/10.1016/S0378-7788\(00\)00114-6](https://doi.org/10.1016/S0378-7788(00)00114-6).
- [60] Naboni E, Natanian J, Brizzi G, Florio P, Chokhachian A, Galanos T, et al. A digital workflow to quantify regenerative urban design in the context of a changing climate. *Renew Sust Energ Rev* 2019;113:109255. <https://doi.org/10.1016/j.rser.2019.109255>.
- [61] Koo C, Hong T, Lee M, Kim J. An integrated multi-objective optimization model for determining the optimal solution in implementing the rooftop photovoltaic system. *Renew Sust Energ Rev* 2016;57:822–37. <https://doi.org/10.1016/j.rser.2015.12.205>.
- [62] Hong T, Kim J, Lee M. A multi-objective optimization model for determining the building design and occupant behaviors based on energy, economic, and environmental performance. *Energy* 2019;174:823–34. <https://doi.org/10.1016/j.energy.2019.02.035>.
- [63] Unzeta BB. Study and prediction of the energy interactions between buildings and the urban climate.Diss. Massachusetts Institute of Technology; 2012. <http://hdl.handle.net/1721.1/77774>.
- [64] Lemercier CAG. Sensitivity analysis of urban Heat Island parameters based on urban weather generator model. Análisis de sensibilidad de los parámetros que influyen en la Isla de calor urbana con el modelo urban weather generator. 2019.
- [65] Palme M, Lobato A, Carrasco C. Quantitative analysis of factors contributing to urban heat island effect in cities of Latin-American Pacific coast. *Procedia Eng* 2016;169:199–206. <https://doi.org/10.1016/j.proeng.2016.10.024>.
- [66] Banishehmi F, Reitberger R, Lang W. Investigating urban Heat Island and vegetation effects under the influence of climate change in early design stages, Sydney, Australia. 2022. p. 679–88. <https://doi.org/10.52842/conf.caadria.2022.2.679>.
- [67] Perini K, Magliocco A. Effects of vegetation, urban density, building height, and atmospheric conditions on local temperatures and thermal comfort. *Urban For Urban Green* 2014;13:495–506. <https://doi.org/10.1016/j.ufug.2014.03.003>.
- [68] Ng E, Chen L, Wang Y, Yuan C. A study on the cooling effects of greening in a high-density city: An experience from Hong Kong. *Build Environ* 2012;47:256–71. <https://doi.org/10.1016/j.buildenv.2011.07.014>.
- [69] Tan Z, Lau KK-L, Ng E. Urban tree design approaches for mitigating daytime urban heat island effects in a high-density urban environment. *Energ Build* 2016;114:265–74. <https://doi.org/10.1016/j.enbuild.2015.06.031>.
- [70] Tang JHG, Lu Z. Use of publicly available data to create a dataset for data-driven urban commercial building energy intensity classification: model accuracy, interpretation, and implications of an open data framework in Hong Kong. *Sustain Cities Soc* 2024;100:105063. <https://doi.org/10.1016/j.scs.2023.105063>.
- [71] Jing R, Wang M, Zhang R, Li N, Zhao Y. A study on energy performance of 30 commercial office buildings in Hong Kong. *Energ Build* 2017;144:117–28. <https://doi.org/10.1016/j.enbuild.2017.03.042>.
- [72] Dai HK, Shi Y, Chen C. Developing a deep neural network model for predicting ventilation rates in public housing buildings in Hong Kong. *Energ Build* 2024;307:113993. <https://doi.org/10.1016/j.enbuild.2024.113993>.
- [73] Ma YX, Yu AC. Impacts of urban heat island on high-rise residential building cooling energy demand in Hong Kong. *Energ Build* 2024;114127. <https://doi.org/10.1016/j.enbuild.2024.114127>.
- [74] Liang H, Shen J, Yip H-L, Fang MM, Dong L. Unleashing the green potential: assessing Hong Kong's building solar PV capacity. *Appl Energy* 2024;369:123567. <https://doi.org/10.1016/j.apenergy.2024.123567>.
- [75] Zimmerman R, Panda A, Bulović V. Techno-economic assessment and deployment strategies for vertically-mounted photovoltaic panels. *Appl Energy* 2020;276:115149. <https://doi.org/10.1016/j.apenergy.2020.115149>.

- [76] On Y, Kim S, Kim S. Multi-objective optimization for design of an agrophotovoltaic system under non-dominated sorting genetic algorithm II. *Comput Electron Agric* 2024;224:109237. <https://doi.org/10.1016/j.compag.2024.109237>.
- [77] Takkanon P. UHI and thermal performance of office buildings in Bangkok. *Procedia Eng* 2017;180:241–51. <https://doi.org/10.1016/j.proeng.2017.04.183>.
- [78] Xu S, Li G, Zhang H, Xie M, Mendis T, Du H. Effect of block morphology on building energy consumption of office blocks: a case of Wuhan. *China Build* 2023;13:768. <https://doi.org/10.3390/buildings13030768>.
- [79] Xie M, Wang M, Zhong H, Li X, Li B, Mendis T, et al. The impact of urban morphology on the building energy consumption and solar energy generation potential of university dormitory blocks. *Sustain Cities Soc* 2023;96:104644. <https://doi.org/10.1016/j.scs.2023.104644>.
- [80] An Y, Chen T, Shi L, Heng CK, Fan J. Solar energy potential using GIS-based urban residential environmental data: a case study of Shenzhen. *China Sustain Cities Soc* 2023;93:104547. <https://doi.org/10.1016/j.scs.2023.104547>.
- [81] Zhao K, Gou Z. Influence of urban morphology on facade solar potential in mixed-use neighborhoods: block prototypes and design benchmark. *Energ Build* 2023; 297:113446. <https://doi.org/10.1016/j.enbuild.2023.113446>.
- [82] Li J, Cui X, Yang J. Multi-scale correlation analysis between geometric parameters and solar radiation in high density urban environment—case study in Nanjing. *Front Archit Res* 2024;S2095263524001079. <https://doi.org/10.1016/j.foar.2024.07.009>.
- [83] Xie M, Wang M, Zhong H, Li X, Li B, Mendis T, et al. The impact of urban morphology on the building energy consumption and solar energy generation potential of university dormitory blocks. *Sustain Cities Soc* 2023;96:104644. <https://doi.org/10.1016/j.scs.2023.104644>.
- [84] Loeffler R, Österreicher D, Stoeglehner G. The energy implications of urban morphology from an urban planning perspective – a case study for a new urban development area in the city of Vienna. *Energ Build* 2021;252:111453. <https://doi.org/10.1016/j.enbuild.2021.111453>.
- [85] Leng H, Chen X, Ma Y, Wong NH, Ming T. Urban morphology and building heating energy consumption: evidence from Harbin, a severe cold region city. *Energ Build* 2020;224:110143. <https://doi.org/10.1016/j.enbuild.2020.110143>.
- [86] Bueno B, Roth M, Norford L, Li R. Computationally efficient prediction of canopy level urban air temperature at the neighbourhood scale. *Urban Clim* 2014;9:35–53. <https://doi.org/10.1016/j.uclim.2014.05.005>.
- [87] Chen L, Zheng X, Yang J, Yoon JH. Impact of BIPV windows on building energy consumption in street canyons: model development and validation. *Energ Build* 2021;249:111207. <https://doi.org/10.1016/j.enbuild.2021.111207>.
- [88] Chen L, Yang J, Li P. Modelling the effect of BIPV window in the built environment: uncertainty and sensitivity. *Build Environ* 2022;208:108605. <https://doi.org/10.1016/j.buildenv.2021.108605>.
- [89] Tian W, Wang Y, Xie Y, Wu D, Zhu L, Ren J. Effect of building integrated photovoltaics on microclimate of urban canopy layer. *Build Environ* 2007;42: 1891–901. <https://doi.org/10.1016/j.buildenv.2006.02.022>.
- [90] Zhou Q, Dong P, Li M, Wang Z. Analyzing the interactions between photovoltaic system and its ambient environment using CFD techniques: a review. *Energ Build* 2023;296:113394. <https://doi.org/10.1016/j.enbuild.2023.113394>.
- [91] Zhang R, Lee M, Huang L. Grid parity analysis of photovoltaic systems considering feed-in tariff and renewable energy certificate schemes in Hong Kong. *Renew Sust Energ Rev* 2023;181:113326. <https://doi.org/10.1016/j.rser.2023.113326>.
- [92] Zhang R, Lee M. Optimization of feed-in tariff mechanism for residential and industrial photovoltaic adoption in Hong Kong. *J Clean Prod* 2023;406:137043. <https://doi.org/10.1016/j.jclepro.2023.137043>.
- [93] Suri M, Betak J, Rosina K, Chrkavy D, Suriova N, Cebecauer T, Caltik M, Erdelyi B. *Global Photovoltaic Power Potential by Country (English)*. Energy Sector Management Assistance Program (ESMAP). Washington, D.C: World Bank Group; 2020. <http://documents.worldbank.org/curated/en/46633159281772524/Global-Photovoltaic-Power-Potential-by-Country>.
- [94] Lou J, Wang B, Yuan Z, Lu W. Willingness to pay for well-being housing attributes driven by design layout: evidence from Hong Kong. *Build Environ* 2024;251: 111227. <https://doi.org/10.1016/j.enbuild.2024.111227>.
- [95] Guidelines on performance-based building energy code. 2007. EDITION. EMSD. https://www.emsd.gov.hk/filemanager/en/content_725/PBBEC_Guide_lines_2007.pdf. (accessed June 30, 2024).